Sensitivity of Near-Surface Variables in the RUC Land Surface Model in the Weather Research and Forecasting Model

Geng Xia,[1] Tatiana G. Smirnova,[2,3] David D. Turner,[2]
Siwei He,[2,3] Ben Yang,[4] Larry K. Berg,[5] Caroline Draxl[1,6]

1 National Renewable Energy Laboratory
2 National Oceanic and Atmospheric Administration Global Systems Laboratory
3 Cooperative Institute for Research in the Environmental Sciences
4 School of Atmospheric Sciences, Nanjing University
5 Pacific Northwest National Laboratory
6 Renewable and Sustainable Energy Institute

Sensitivity of Near-Surface Variables in the RUC Land Surface Model in the Weather Research and Forecasting Model

Geng Xia,[1] Tatiana G. Smirnova,[2,3] David D. Turner,[2] Siwei He,[2,3] Ben Yang,[4] Larry K. Berg,[5] Caroline Draxl[1,6]

1 National Renewable Energy Laboratory
2 National Oceanic and Atmospheric Administration Global Systems Laboratory
3 Cooperative Institute for Research in the Environmental Sciences
4 School of Atmospheric Sciences, Nanjing University
5 Pacific Northwest National Laboratory
6 Renewable and Sustainable Energy Institute

NOTICE

Acknowledgments

List of Acronyms

RUC	rapid update cycle
LSM	land surface model
WFIP2	Second Wind Forecast Improvement Project
NOAA	National Oceanic and Atmospheric Administration
HRRR	high-resolution rapid refresh
WRF	Weather Research and Forecasting
PS	physics site
MYNN	Mellor–Yamada–Nakanishi–Niino
PBL	planetary boundary layer
QMC	quasi-Monte Carlo
KZERO	thermal conductivity for feldspar
KQWRTZ	thermal conductivity for quartz
KICE	thermal conductivity for ice
KWT	thermal conductivity for water
C1SN	constant for snow density calculations
Melt1	melt factor for other vegetation type
Melt2	melt factor for mixed and evergreen forests
LB	blending height
REFKDT	constant for calculation of max infiltration
AP0	constant for calculation of transpiration function
GLM	generalized linear model
EBBR	energy balance bowen ratio
SH	sensible heat
LH	latent heat
GH	ground heat
LST	land surface temperature
WS100	hub-height wind speed
T2	air temperature at 2 meters

Executive Summary

In this study, we investigate the parametric sensitivity of near-surface variables, such as sensible heat flux, latent heat flux, ground heat flux, hub-height wind speed and land surface temperature, to the parameters used in the rapid update cycle (RUC) land surface model (LSM) during a winter and summer periods. The model simulations are compared with observations collected from the second Wind Forecast Improvement Project (WFIP2) field campaign. The results suggest that parameters related to snow/ice and thermal processes can have significant impact on the simulated near-surface variables. Out of the 11 examined parameters, only 6 have considerable influences on the model behaviors and can explain about 60%–80% of the estimated total variance of the simulated variables. In addition, the magnitude of the parametric sensitivity varies with season. For instance, parameters associated with snow/ice processes are dominant during the wintertime, whereas those associated with thermal processes are more important during the summertime. Furthermore, the impact of the identified parameters on the simulated variables is highly related to the topography. There is a high degree of sensitivity to the parameter values over the slope region. This points out the importance of collecting field observations over steep areas to better quantify the appropriate values of key parameters. Overall, our findings provide a better understanding of the RUC LSM behavior associated with parameter uncertainties and can be used to improve the forecasting skill of land surface processes via calibration of the most uncertain model parameters.

Table of Contents

List of Figures

List of Tables

1 Introduction

Near-surface states, such as temperature, wind speed and energy fluxes, strongly influence the strength of land-atmosphere coupling as they regulate the exchanges of energy, moisture and momentum between the land surface and the overlaying atmosphere. In addition, they act as the lower boundary forcing in the state-of-art Weather Research and Forecasting (WRF) model which ultimately affects thermally and mechanically-driven vertical mixing in the atmospheric boundary layer (Santanello et al. 2018; Findell et al. 2015; Wang et al. 2020). Therefore, it is critical to accurately represent these quantities in the numerical weather prediction.

In the WRF model, the surface energy budget and other near-surface variables are predicted by the land surface model (LSM) based on fundamental physical processes, which are often parameterized with fine-tuned empirical parameters as these processes cannot be explicitly resolved (Mahrt and Pan 1984; Chen et al. 1996; Niu et al. 2011). Even though the values of those parameters are calibrated with observations, there are still large uncertainties as the observational samples used for calibration are often limited in number and mostly idealized. Thus, understanding the uncertainties associated with the parameters in the LSM would be critical to improve land surface predictions which in turn would lead to better numerical forecasting.

One method in this context is sensitivity analysis, which explores the high-dimensional parameter space of a complex model and evaluates the model responses to the input parameters. The biggest advantage of the sensitivity analysis is that it offers an effective way to quantify parameters sensitivities to understand whichever parameter is the most important to the model outcome. As a result, numerous studies have applied such technique to investigate the parameter sensitivity from various schemes in the WRF model (Hou et al. 2012; Yang et al. 2017, 2019; Berg et al. 2021; Liu et al. 2022; Guo et al. 2014; Zhao et al. 2013; Rosero et al. 2010). Over the years, LSM has grown in complexity from a simple thermal model to encompass a broad range of interrelated disciplines including hydrology, ecology, biology, urbanization, and so on (Bastidas et al. 2006; Fisher al et. 2020). It is, therefore, important to conduct the sensitivity analysis to assess the effect of input parameters from LSM on the model outcome.

In this study, we apply the sensitivity analysis framework to examine parameter sensitivity in the rapid update cycle (RUC) LSM. The goal is to identify the most influential parameters on simulated surface properties. The RUC LSM is widely known as the land surface component in the National Oceanic and Atmospheric Administration (NOAA) operational rapid refresh short-range weather prediction model over the North America domain and in the High-Resolution Rapid Refresh (HRRR) model over the continental United States. Therefore, understanding the parameter uncertainty in the RUC LSM would provide critical guidance for model calibration and validation for the next generation of LSM development.

This report is organized as follows: Section 2 describes the WRF configuration, experiment design, targeted parameters, observations used for model validation and the sensitivity analysis framework. Section 3 presents the result discussion including (i) model performance evaluation with the observations; (ii) key LSM parameters that are identified from the sensitivity analysis; (iii) dependence of parametric sensitivity on other factors, such as land-use type and soil category and (iv) the impact of the key LSM parameters on the simulated near-surface variables.

This report is available at no cost from the National Renewable Energy Laboratory at www.nrel.gov/publications.

Section 4 discusses the uncertainty associated with the method and the analysis, followed by a summary of the main findings in Section 5.

2 Data and Methodology

2.1 Simulation Design and Experiment Setup

The simulation design is similar to that employed in Xia et al. (2021; 2022), and the following text is derived from there with minor modifications. The WRF version 4.1.2 (Skamarock and Klemp 2008; Powers et al. 2017) is used to conduct model simulations in this study. The boundary and initial conditions are obtained from the HRRR datasets from the Google Cloud archive (https://console.cloud.google.com/marketplace/product/noaa-public/hrrr?project=python-232920&pli=1).

Two nested domains cover the entire northwestern United States with the inner domain centered on the field campaign region from WFIP2. The outer domain (Figure 1a) consists of 120 × 85 grid points with the horizontal resolution of 9 km while the inner domain (Figure 1b) consists of 145 × 115 grid points with the horizontal resolution of 3 km. There are 52 vertical levels employed with finer resolution at the lower levels and coarser resolution at the higher levels. The black dot at the inner domain indicates the location of the Physics Site 01 (PS01) and PS03 where all the observations for this paper were collected.
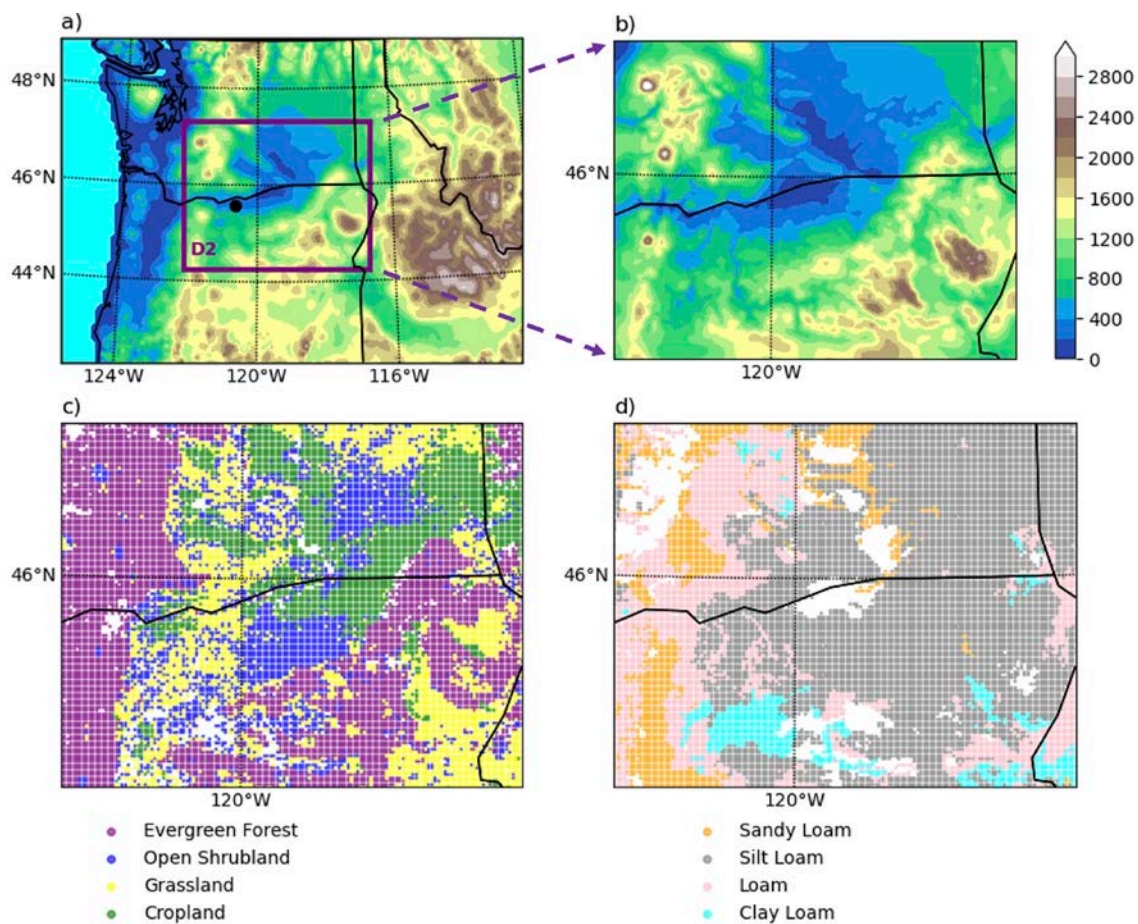
Figure 1. Spatial pattern of topographical maps (m) for the (a) outer domain, (b) inner domain, (c) dominant land-use type and (d) soil category for the inner domain. The black dot in (a) indicates the geographical location of the PS01 and PS03.

3

The physics options used in this study include rapid radiative transfer model for shortwave and longwave radiation (Iacono et al. 2008), Thompson aerosol-awareness microphysics scheme (Thompson et al. 2008; Thompson and Eidhammer 2014), Mellor–Yamada–Nakanishi–Niino (MYNN) level 2.5 planetary boundary layer (PBL) scheme and MYNN surface layer scheme (Mellor and Yamada 1982; Nakanishi and Niino 2009). Note that cumulus convection is treated explicitly for second domain while it is parameterized for the outermost domain using the Kain–Fritsch scheme (Kain and Fritsch 1990, 1993; Kain 2004). The moderate resolution imaging spectroradiometer (MODIS) land-use and default soil datasets are used to set the initial land state and soil category.

Following Yang et al. (2017), the experiment is run using a one-way nesting method where the model output from the outer domain is used as the initial and boundary conditions to drive the inner domain that is performed repeatedly with the perturbed parameter values (see Section 2.2). This strategy helps to isolate the impacts of parameter perturbations within the inner domain (i.e., local impacts) from the changes in boundary forcing. The 128 ensembles of perturbed parameters were generated using the quasi-Monte Carlo (QMC) sampling approach (Caflisch 1998) for two simulation periods, one during the summertime (11−31 July 2016) and the other during the wintertime (21 February to 13 March 2017). Each period has a duration of 20 days to allow the examination of the parameter sensitivity of near-surface variables under two distinctive weather and land surface conditions.

2.2 Parameters From the RUC LSM

The details of the model description for the RUC LSM can be found in Smirnova et al. (1997, 2000, and 2016). In this study, we focused on parameters that could have a significant impact on the soil thermal and hydrology processes. In total, 11 parameters were identified and listed in Table 1. The uncertainty ranges associated with these parameters were determined based on past literatures (Johansen 1975; Kenji 1967; Schaake et al. 1996; Koren et al. 1999) and discussions with the RUC LSM developers. Parameters, such as KZERO, KQWRTZ, KICE, and KWT, are related to soil thermal conductivity that largely influence the land surface temperature and surface heat flux whereas other parameters like C1SN, C2SN, melt factors, REFKDT, and AP0 are associated with hydrological processes like snow/ice melting and soil moisture infiltration. Note that melt factor indicates the speed of snow melting. In general, the smaller the value is, the longer the snow stays on the land surface. The last examined parameter, LB, is used to compute the time varying roughness length, which would be important for wind speed calculation. Since thermal conductivity is often measured and is subjected to less uncertainty, the perturbed range for parameters associated with thermal conductivity are smaller (± 10 %) compared to the other parameters (± 50 %). The uncertainty associated with the parameter values is discussed in Section 4.

Table 1. Investigated Parameters in the RUC LSM

Parameters	Description	Default Value	Range
KZERO	Thermal conductivity for feldspar(W.m^{-1}K^{-1})	2.0	1.9–2.1
KQWRTZ	Thermal conductivity for quartz (W.m^{-1}K^{-1})	7.7	7.31–8.09
KICE	Thermal conductivity for ice (W.m^{-1}K^{-1})	2.2	2.09–2.31
KWT	Thermal conductivity for water (W.m^{-1}K^{-1})	0.57	0.54–0.60
C1SN	Constant for snow density calculations	0.026	0.013–0.039
C2SN	Constant for snow density calculations	21	10–31
Melt factor 1 (Melt1)	Melt factor for other vegetation types	2	1.0–3.0
Melt factor 2 (Melt2)	Melt factor for mixed and evergreen forests	0.85	0.4–1.3
LB	Blending height	5.0	2.5–7.5
REFKDT	Constant for calculation of max infiltration	3.0	1.5–4.5
AP0	Constant for calculation of transpiration function	0.299	0.15–0.45

2.3 Sensitivity Analysis Framework

Following Yang et al. (2017), the sensitivity analysis framework applied in this study can be summarized in three steps. The first step is to identify the most relevant parameters from the RUC LSM. The second step is to sufficiently sample points using the QMC approach to perturb the identified parameters into 128 perturbed ensembles (Hou et al. 2012). Those perturbed parameters are then used to create the model ensemble needed for the third step. In the third step, the sensitivity analysis is applied to the model output using a variance-based approach. For that, the sensitivity of an input parameter is determined by its contribution to the total variance of the model output. The generalized linear model (GLM; McCullagh and Nelder 1989) is constructed for that purpose and is used to examine the parameter sensitivity as well as parameter impacts on the simulated near-surface variables from the model ensemble using Eq. 1:

$$V = \beta_0 + \sum_{j=1}^{n} \beta_j * P_j + \sum_{j=1}^{n} \beta_j * P_j^2 + \sum_{j=1}^{n} \sum_{k=1}^{n} \beta_{j,k} * P_j * P_k + \varepsilon \qquad (1)$$

where P_j and P_k represent the value of the jth and k^{th} parameter, respectively. β_j and $\beta_{j,k}$ represent the coefficients of linear and quadratic ($j = k$) or two-way interaction ($j \neq k$) terms, respectively. β_0 is the interception and δ denotes the residual. Therefore, the second, third, fourth and fifth term on the right-hand side of the equation represents the contribution from the parameter terms, quadratic terms, interactive term and residual term, respectively, to the total estimated variance.

2.4 WFIP2 Observations

To validate the model simulation with the observations, the surface temperature measurement and flux measurement from the PS03 and PS01 are used (Shaw et al. 2019; Wilczak et al. 2019). The energy balance bowen ratio (EBBR) system from PS03 is used to collect surface measurements such as sensible heat flux (SH), latent heat flux (LH), ground heat flux (GH), and surface temperature (LST). The hub-height wind speed (WS100) and air temperature at 2 m (T2) are collected from the Vaisala Triton SoDAR wind profiler (Vaisala 2015), respectively, at PS01.

5

All the raw data are quality-controlled and compiled into hourly averages. Details about instrumentation, data quality and data uncertainty can be found in Cook and Sullivan (2018) and Xia et al. (2021).

3   Results

3.1   Validating Simulated Near-Surface Variables With the Observations

The overall performance of the parametric perturbation experiments can be evaluated by comparing simulated near-surface variables with the observations collected from the WFIP2 field campaign. During the summertime (Figure 2), there is general good agreement between the model and observations for WS100, SH flux and T2 in terms of both magnitude and timing. However, the simulations fail to predict the maximum value of the observed SH flux (~500 W.m^{-2}) during daytime. Note that the observed LH flux is more variable compared with the simulated SH flux. That is due to the measurement uncertainty from the ERRR when there is limited soil moisture in the ground (Cook and Sullivan 2018; Xia et al. 2022). Similar to Xia et al. (2021), the modeled GH flux show the largest discrepancy as compared with the observations which is associated with the cold bias in the simulated LST. Interestingly, the simulated T2 agrees very well with the observations, suggesting that the error in simulating LST could be a dominant factor in calculating the near-surface thermal gradient and thus could have a potential impact on the mixing mechanisms in the PBL scheme. During the wintertime (Figure 3), almost all the near-surface variables show a lesser agreement and larger variability compared with the observations. That is most likely due to the difficulty in accurately capturing the winter disturbances such as the frontal passage and cold cool over this region during this period (McCaffrey et al. 2019; Bianco et al. 2019; Pichugina et al. 2020). However, the simulated LH flux does correspond better than the observed measurement and the cold bias in the simulated LST is significantly smaller as compared to that from the summertime.
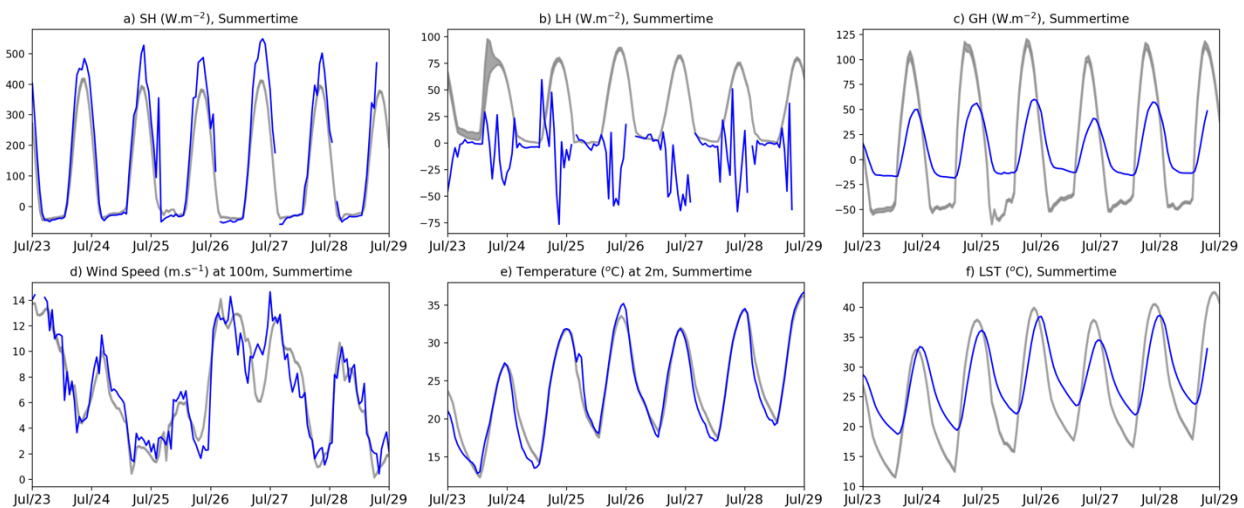
Figure 2. Time series of the observed (blue) and simulated (gray) (a) SH flux, (b) LH flux, (c) GH flux, (d) WS100, (e) T2, and (f) LST during the summertime period from 23 to 29 July 2016. The gray shaded area indicates the ensemble range.

7
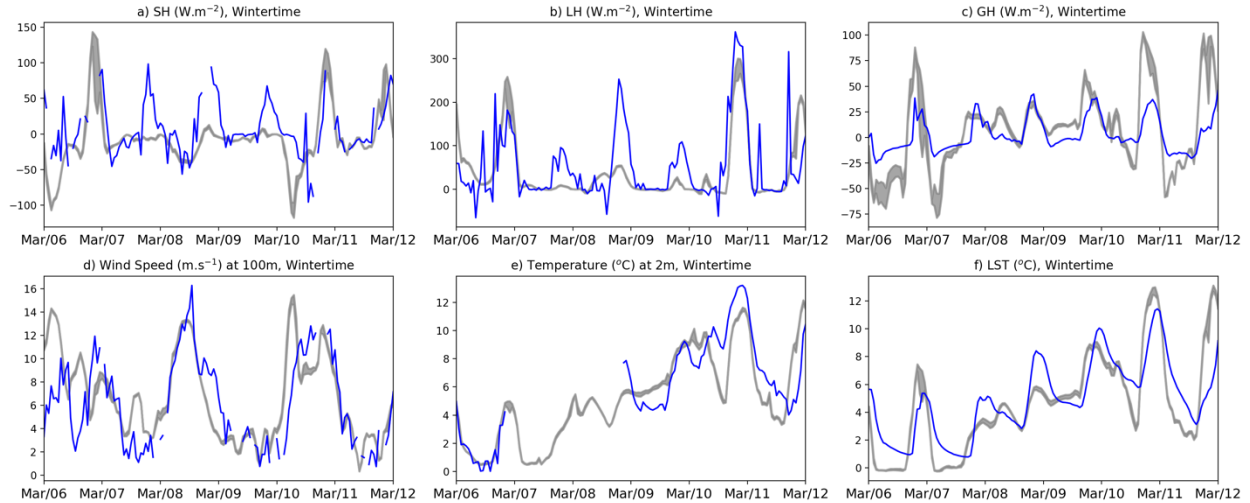
Figure 3. Same as Figure 2 but for wintertime period from 6 to 12 March 2017.

The simulated ranges for all the near-surface variables from the perturbation experiments are generally small during the summertime compared to the wintertime. However, that is just for one location where the topography is relatively flat without much geological heterogeneity (Figure 1b). Therefore, we calculate the standard deviation at each point for the entire domain 2 to illustrate the spatial variability of the ensemble spread. During the summertime (Figure 4), the standard deviation for each simulated variable is rather weak and uniform across the entire region, except for certain high-terrain areas. For instance, Mount Rainier, the high volcanic peak located at the northwestern side of the map, shows the highest parametric sensitivity for all the variables. During the wintertime (Figure 5), the spatial characteristic of standard deviation of each simulated variable is more variable and exhibits a stronger magnitude than in the summertime. Interestingly, the ensemble spread for WS100 is rather small regardless of the geography and season. This suggests that the impact of LSM parameters on the simulated hub-height wind speed is limited as compared to the that from the PBL and surface layer scheme (Yang et al. 2017, Berg et al. 2019; 2021). As for the other variables (SH, LH, GH, T2, and LST), the ensemble spread is greater over the wintertime than over the summertime, particularly, over regions with high elevation and steep slope. This indicates that parametric sensitivity for the near-surface variables is strongly associated with seasonality and geological heterogeneity.

8
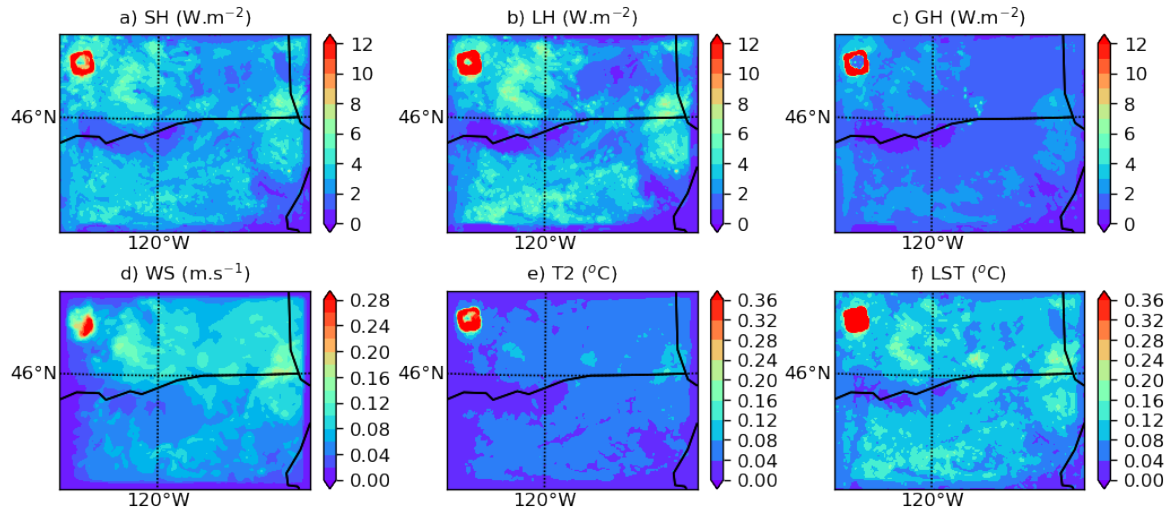
Figure 4. Spatial pattern of the intermember standard deviation for the simulated (a) SH, (b) LH, (c) GH, (d) WS100, (e) T2, and (f) LST for the summertime period (11−31 July 2016)
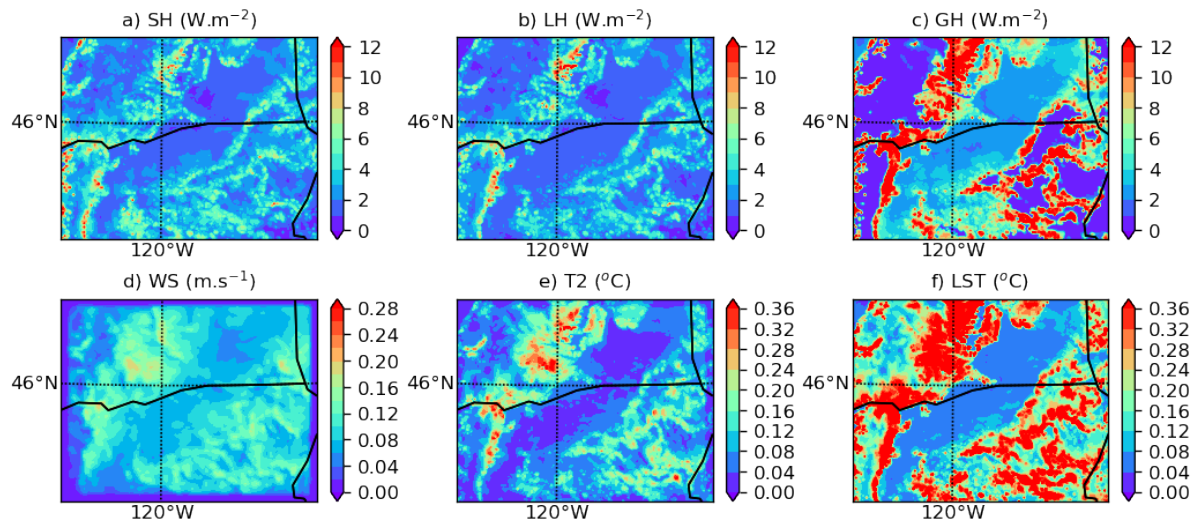
Figure 5. Same as Figure 4 but for the wintertime period (12 February to 13 March 2017)

To further understand the variance induced by the parameter perturbation, Tables 2 and 3 show the fraction of variance explained by the four representative terms from the GLM analysis (Eq.1) during midday (10 a.m. to 2 p.m.) and midnight (10 p.m. to 2 a.m.) for both summer and winter periods, respectively. During the summertime, the parametric term on a domain average contributes about 30% of the total variance for all the variables. This suggests that the parametric sensitivity for the near-surface variable is relatively weak over the summertime. Interestingly, its contribution drastically increases to about 65% during the winter period. The drastic contrast between summer and winter indicates that the parametric sensitivity for RUC LSM varies with season. In addition, the parameter contribution to the total variance is generally smaller during midday than midnight, possibly due to the strong land-atmosphere coupling in the daytime.

9

The relative contribution of each examined parameter (Table1) to the total variances is explored in more detail in the following section.

Table 2. Fraction of Variance of the Simulated Near-Surface Variables Explained by the GLM for Summertime (11−31 July 2016)

	Daytime					Nighttime			
	Parameters	**Quadratic**	**Interactive**	**Residual**		**Parameters**	**Quadratic**	**Interactive**	**Residual**
SH	18%	7%	38%	35%		32%	6%	21%	20%
LH	14%	8%	40%	37%		17%	8%	39%	36%
GH	53%	4%	22%	20%		45%	5%	26%	23%
WS100	37%	7%	28%	26%		29%	7%	33%	31%
T2	35%	6%	30%	28%		58%	4%	19%	18%
LST	26%	7%	34%	32%		53%	4%	21%	20%

Table 3. Fraction of Variance of the Simulated Near-Surface Variables Explained by the GLM for Wintertime (21 February to 13 March 2017)

	Daytime					Nighttime			
	Parameters	**Quadratic**	**Interactive**	**Residual**		**Parameters**	**Quadratic**	**Interactive**	**Residual**
SH	54%	8%	20%	17%		58%	10%	18%	15%
LH	58%	9%	18%	16%		57%	9%	18%	15%
GH	48%	11%	24%	17%		42%	9%	18%	15%
WS100	75%	8%	9%	8%		72%	9%	10%	8%
T2	72%	7%	11%	10%		66%	8%	14%	11%
LST	63%	7%	16%	14%		59%	9%	17%	14%

3.2 Sensitivity of the Near-Surface Variables to the Parameters From the RUC LSM

As discussed in Section 2.3, the generalized linear model is applied to decompose the total variances into portions contributed by individual parameter, higher order, and interaction terms. To understand the spatial feature of the parametric sensitivity, we apply the GLM analysis at each model grid of the inner domain. Figure 6 shows the spatial pattern of the relative contribution of the 11 parameters to the variance of the simulated WS100 for both summer and winter periods. To avoid figure redundancy, the result is the average over both daytime and nighttime. Even though the day-night contrast of the parametric sensitivity is not explicitly discussed in this paper, it will be briefly mentioned in the uncertainty section (Section 4). As shown in Figure 6 the blending height (LB) is the most consistent contributing factor to the total variance of WS100 for both the summer and winter periods whereas the sensitivity to the melting factors (Melt1 and Melt2) increases drastically during the winter period.

In addition, there is some dependence on the terrain height where the parametric sensitivity is generally high over the mountain region and small over the Columbia Basin. Similar studies (Yang et al. 2017; Berg et al. 2019 and 2021) have been done using parameters from the PBL scheme. Comparing their results with this study, the analysis suggests that the impact of LSM parameters on the variability of hub-height wind speed is generally weaker than that from the PBL parameters.

The results for the surface energy fluxes are shown in Figure 7 (SH), Figure 8 (LH) and Figure 9 (GH). Notably, the sensitivity of LB has dropped significantly for all the surface fluxes for both simulation periods. During the summertime, the parametric sensitivity to the surface energy fluxes is generally small, suggesting that the processes contributing to the total variance are largely nonlinear. Even so, parameters associated with the thermal conductivity, such as KWT, KZERO and KQWRTA, can contribute up to ~30 % of the total variance despite their relatively small perturbation range ($\pm$5% of the default value). During the wintertime, Melt1 and Melt2 are still the most dominating contributors. In addition, the strength of sensitivity shows a strong dependency on the geographical location. This indicates that the parametric sensitivity from the LSM is related to the land-use type and soil category which will be further discussed in the next section. The results for LST (Figure 10) and T2 (Figure 11) illustrate the similar characteristic of the relative contribution. In general, parameters associated with snow and ice processes are dominant over the wintertime whereas parameters associated with thermal conductivity are more influential during the summertime. Based on the discussion above, six key RUC LSM parameters (Melt1, Melt2, KWT, KZERO, KQWRTZ, and LB) are identified and later analysis will only focus on these six key parameters, unless otherwise mentioned.

11
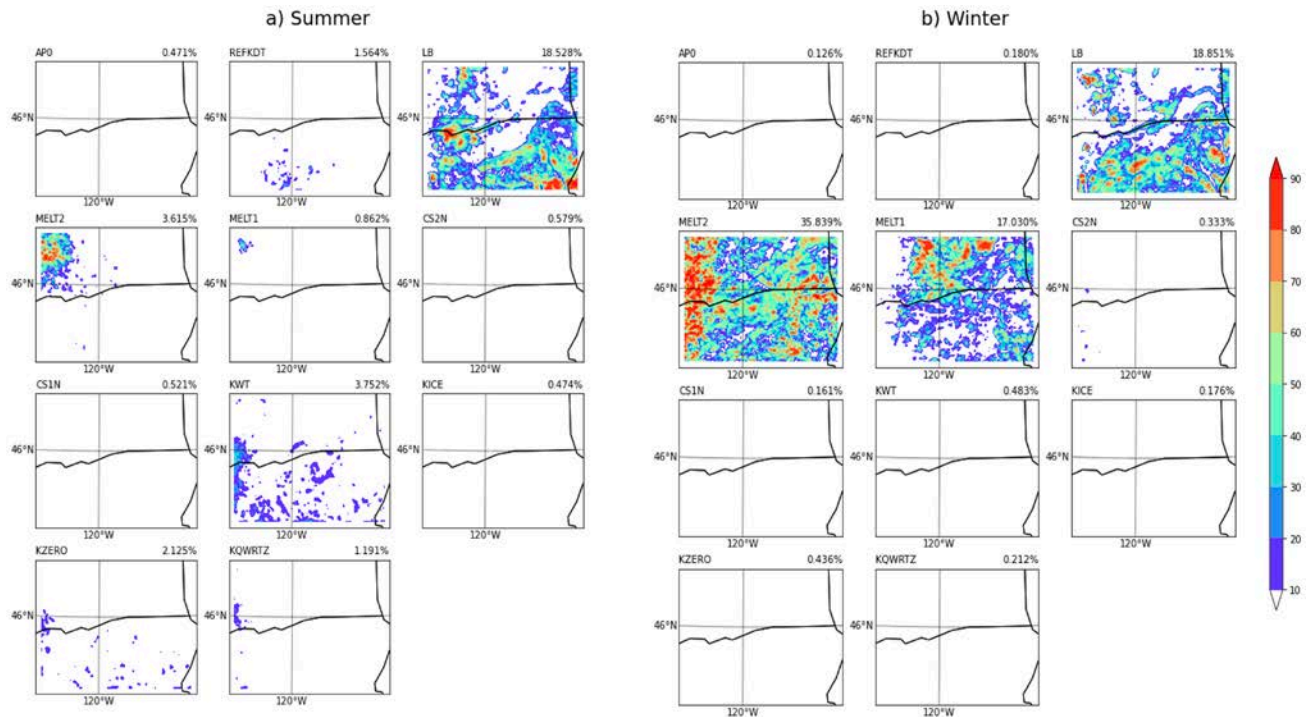
Figure 6. Spatial distributions of relative contributions (%) of each examined parameter (Table 1) to the total variances of the simulated WS100 during (a) summertime and (b) wintertime
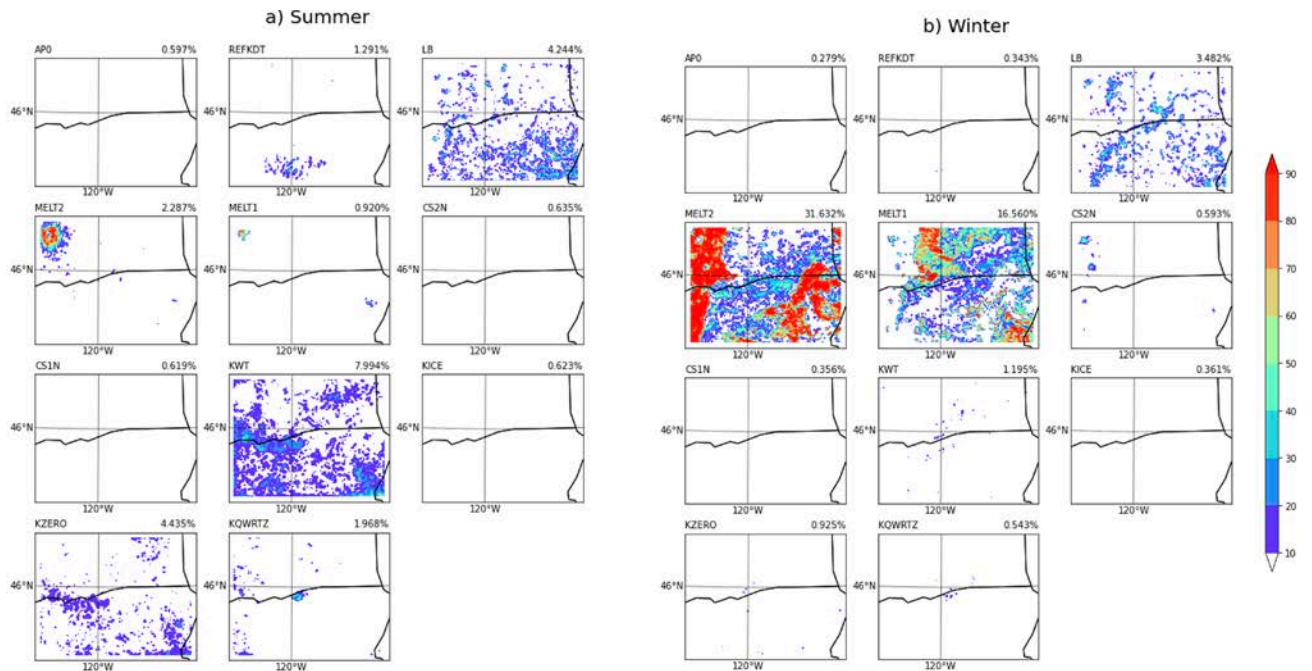
Figure 7. Same as Figure 6 but for simulated SH flux

12
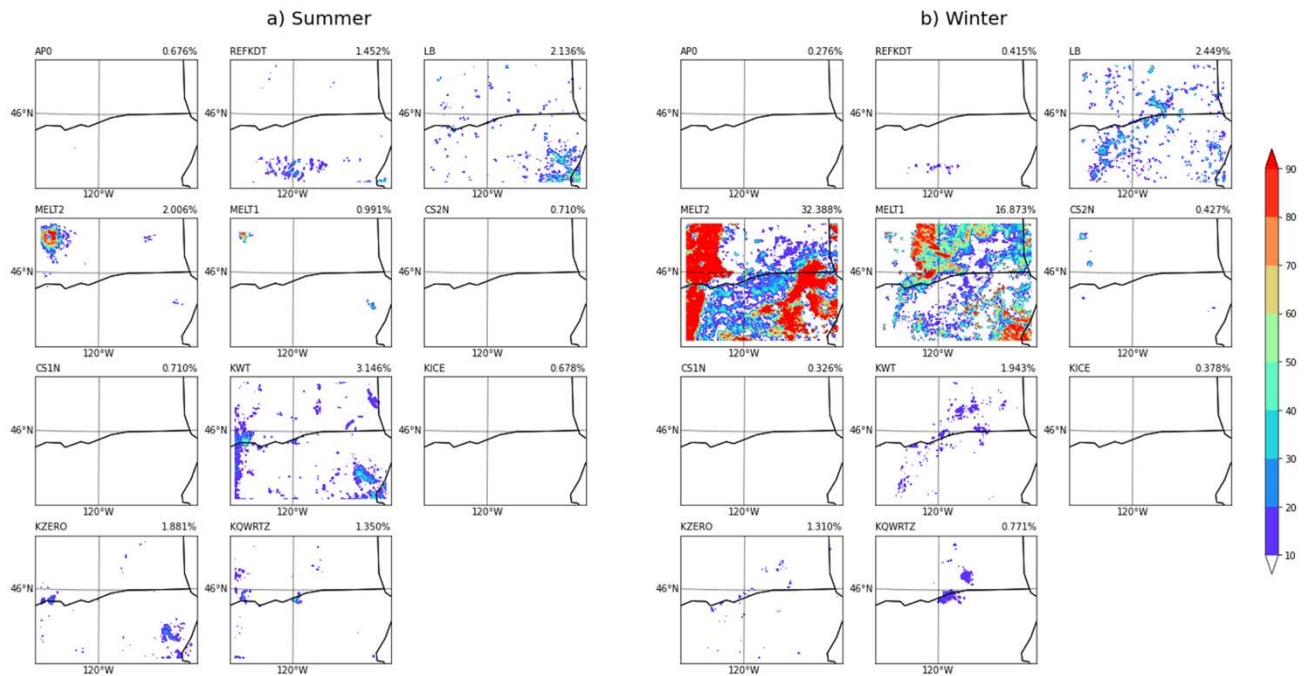
Figure 8. Same as Figure 6 but for simulated LH flux
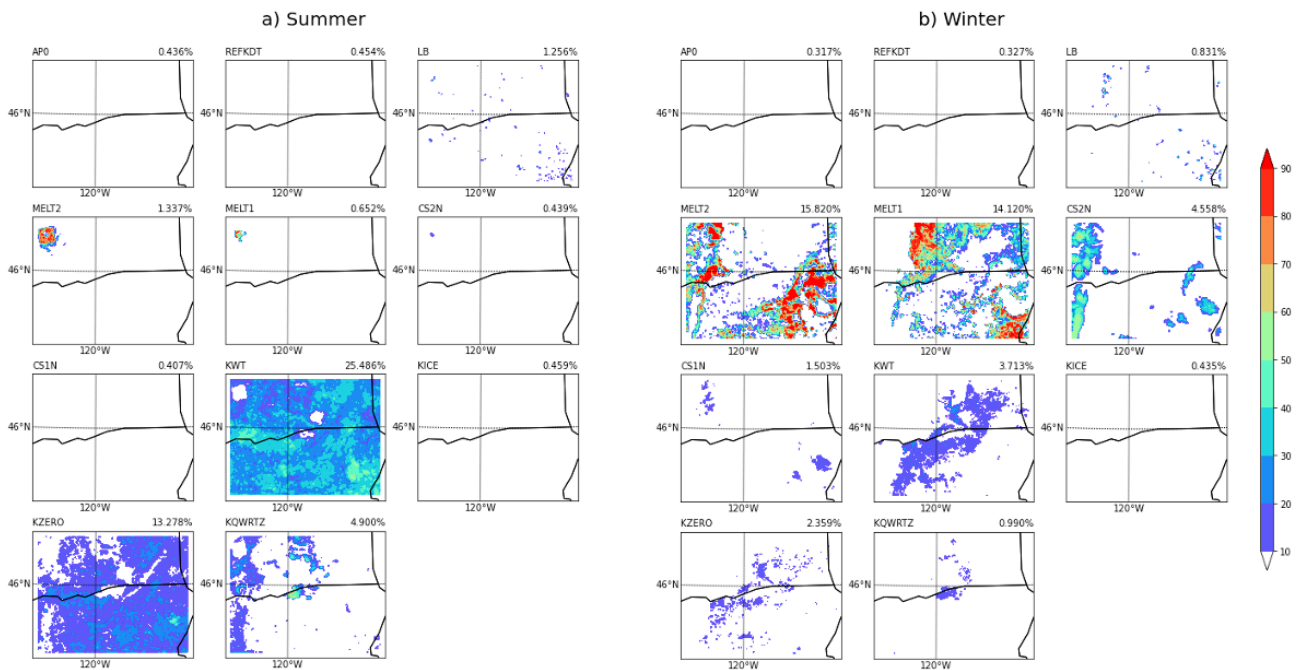
Figure 9. Same as Figure 6 but for simulated GH flux

13
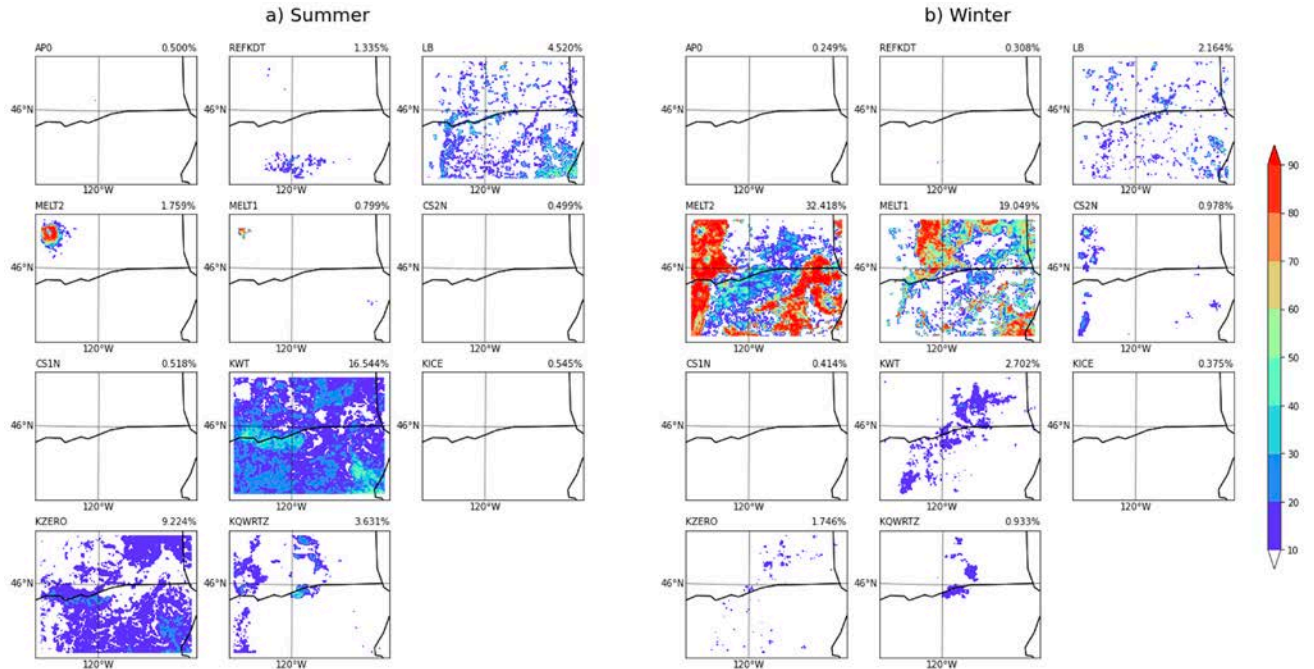
Figure 10. Same as Figure 6 but for simulated LST
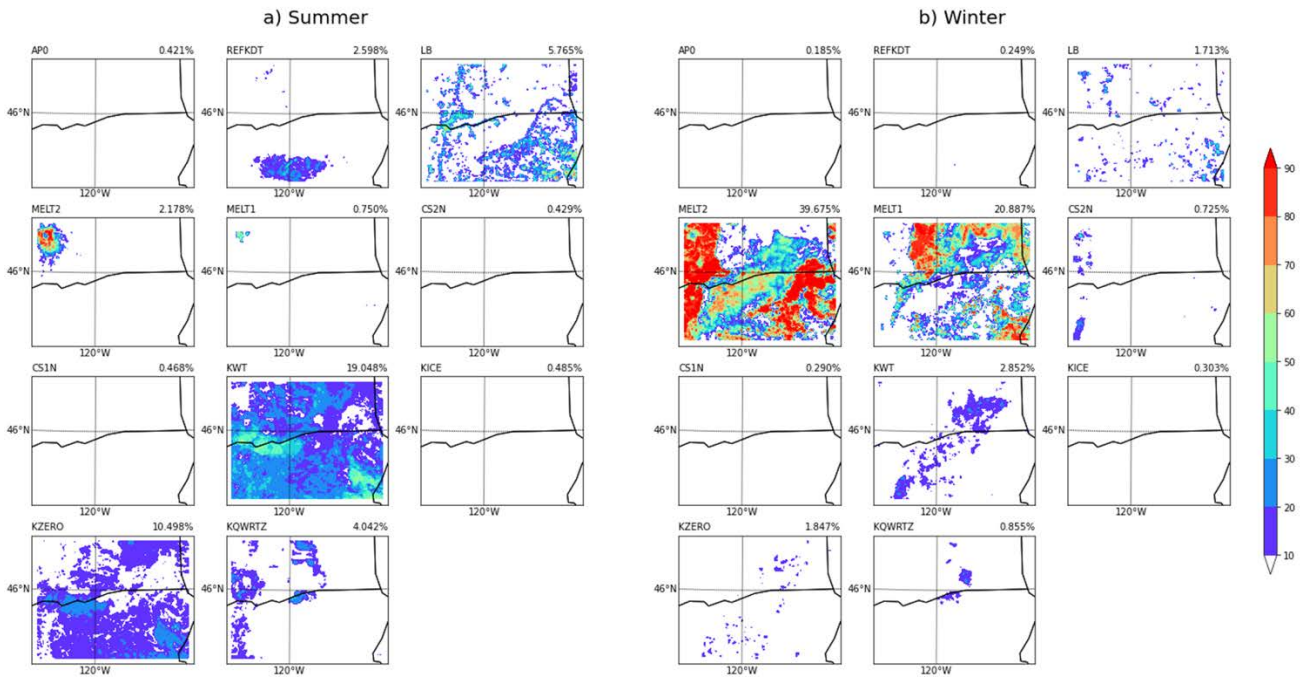
Figure 11. Same as Figure 6 but for simulated T2

14

3.3 Dependence on Land-Use Type and Soil Texture

The land surfaces states, such as soil texture and land-use type, play a major role in determining the surface roughness length and flux (e.g., energy, momentum, and moisture) transfer. Therefore, it is important to understand the dependence of land-use and soil category on the parametric sensitivity of the near-surface variables over the simulation domain. In our simulation, there are 20 land-use types and 16 soil textures. Within the inner domain, four different land-use types (evergreen forest, open shrubland, grassland, and crop land) and soil textures (sandy loam, silt loam, loam, and clay clam) represent the surface condition for over 90% of the total pixels (Figures 1c and 1d). Thus, we categorize the parametric sensitivity of the six key parameters over these four dominant land-use and soil categories for both simulation periods.

For all the simulated variables (Figures 12, 13, 14, and 15), the relative contribution to the total variances is much higher over the wintertime than summertime regardless of the land-use and soil categories. In addition, the variation in the relative contribution over each land-use type and soil texture is negligible during the summertime. However, the relative contribution for most variables (e.g., SH, LH, LST, and T2) is generally higher over the evergreen forest region than the other land-use types during the wintertime due to the significant contribution from Metl2 (Figure 12 and Figure 14). No significant variation is apparent over the different soil textures (Figure 13 and Figure 15). As for individual parameters, similar to what we have discussed in the previous section, the parameter associated with surface roughness (LB) is the most consistent contributing factor to the simulated hub-height wind speed. Parameters associated with melting processes are highly sensitive during the wintertime whereas the parameters associated with thermal processes contributes more to the variability during the summertime. This is true regardless of whichever land-use and soil categories, which suggests that there is little dependence on the land-use type and soil textures to the parametric sensitivity from the RUC LSM.

This report is available at no cost from the National Renewable Energy Laboratory at www.nrel.gov/publications.
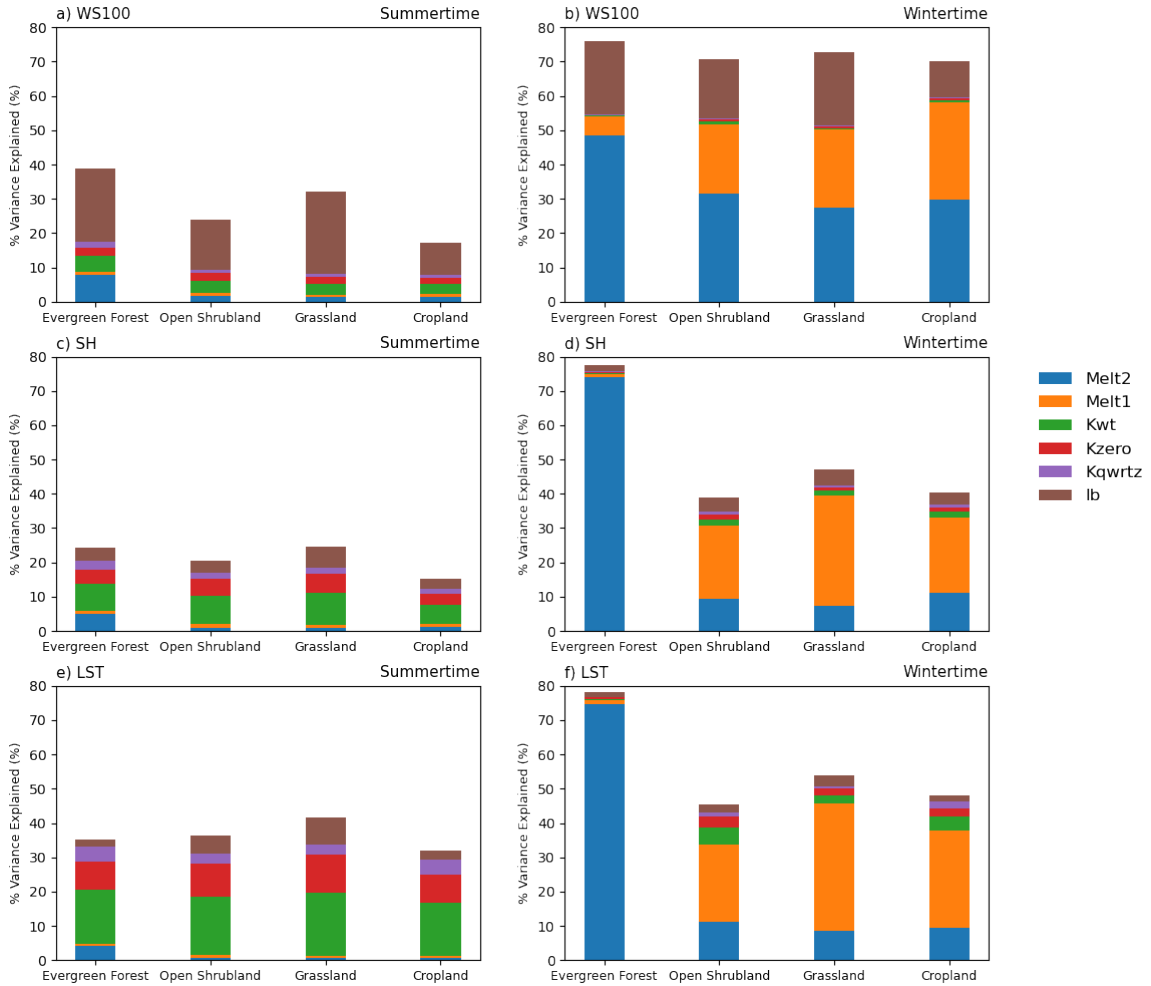
Figure 12. The relative contribution of the six key parameters (Melt1, Melt2, KWT KZERO, KQWRTZ, and LB) to the variance of (a, b) WS100, (c, d) SH, and (e, f) LST with respect to the four dominant land-use types (evergreen forest, open shrubland, grassland, and cropland) for both the summer (left) and winter (right) periods

16
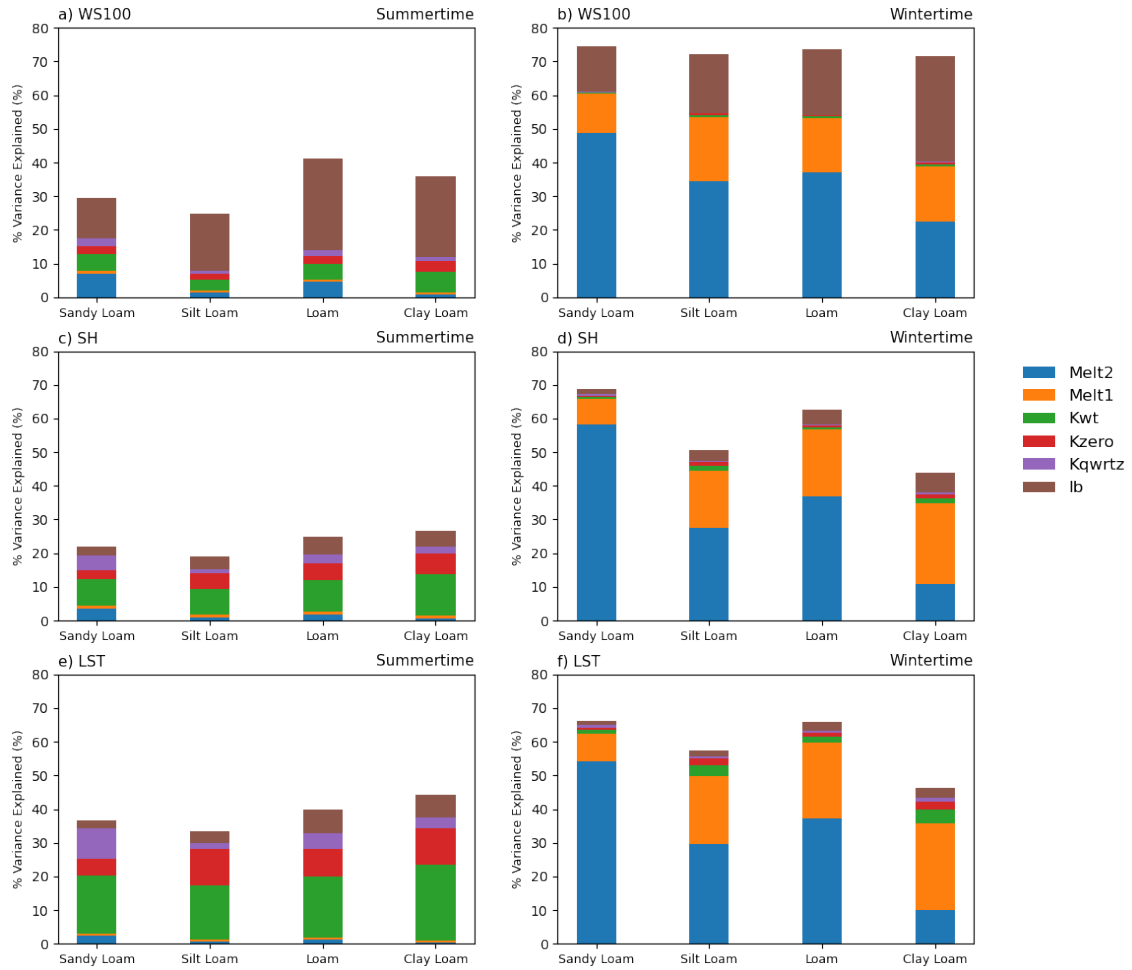
Figure 13. Same as Figure 12 but with respect to the four dominant soil textures (sandy loam, silt loam, loam, and clay loam)
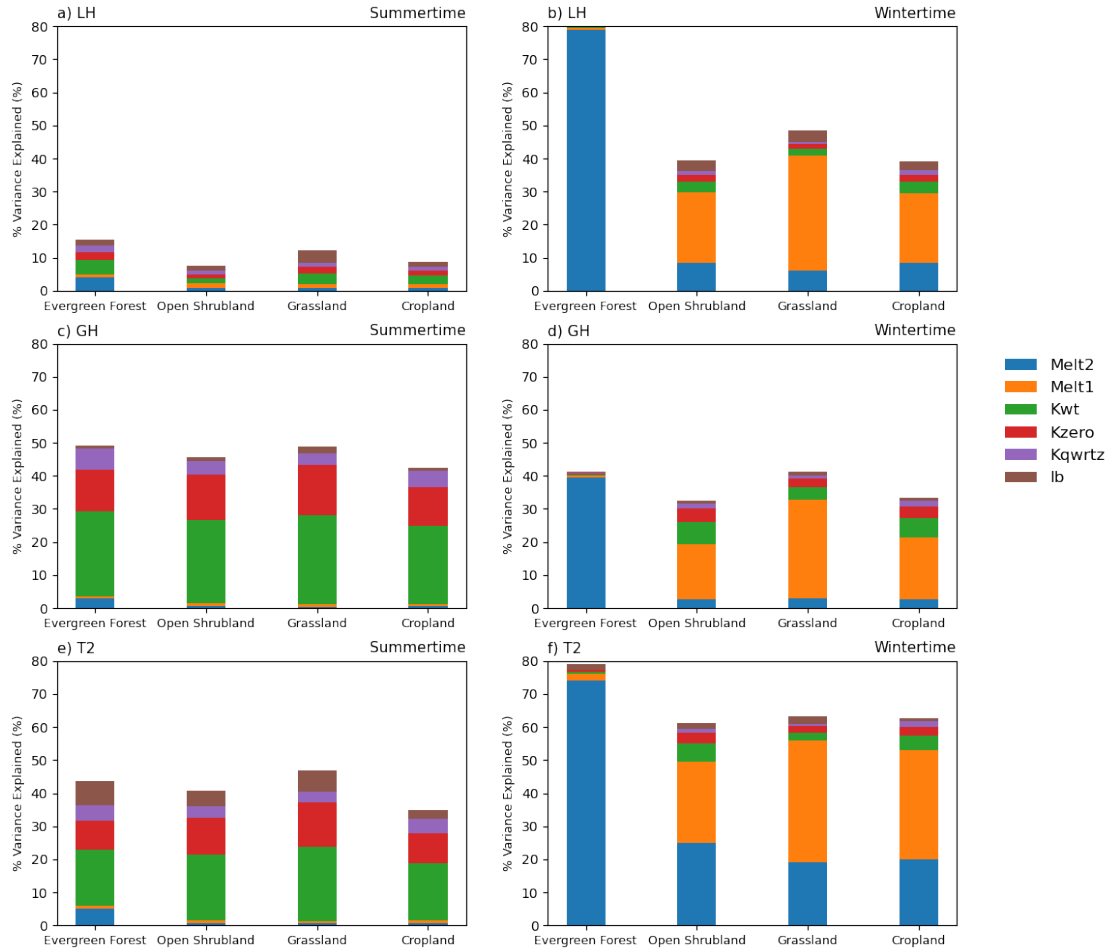
Figure 14. The relative contribution of the six key parameters (Melt1, Melt2, KWT, KZERO, KQWRTZ, and LB) to the variance of (a, b) LH, (c, d) GH, and (e, f) T2 with respect to the four dominant land-use types (evergreen forest, open shrubland, grassland, and cropland) for both (left) summertime and (right) wintertime

18
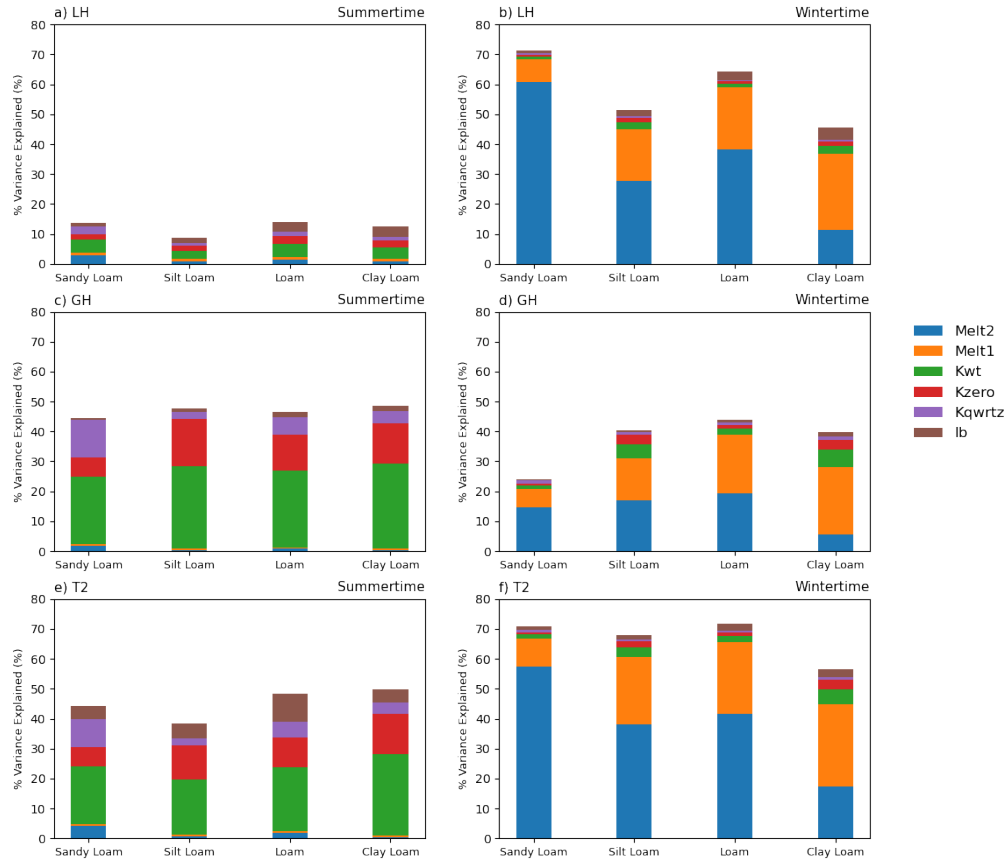
Figure 15. Same as Figure 14 but with respect to the four dominant soil categories (sandy loam, silt loam, loam, and clay loam)

3.4 Quantify the Sensitivity of the Key Parameters on the Simulated Near-Surface Variables

Previous discussion has identified the six key parameters from the RUC LSM that are responsible for the variability of the simulated near-surface variables from the parameter perturbation experiments. However, the responses (e.g., positive or negative) of the simulated near-surface variables to each parameter is still unknown. To quantify the response, two groups of simulations are subcategorized from the original 128 ensemble for each parameter. One group consists of model simulations with high values of the parameter (> 75th percentile) while the other group has the simulations with low values (< 25th percentile). As a result, each group consists of 32 model ensemble members. Therefore, the response of simulated variables to each parameter is examined by calculating the difference between the two ensembles with the assumption that the impact from the other parameters will be largely canceled out due to the nature of random sampling.

Figure 16 shows the response of simulated WS100 to the six key parameters for both the summer and winter periods. Evidently, the LB parameter has a consistent positive impact on WS100 for both simulation periods. This indicates that an increase in LB would increase the simulated hub-height wind speed. The other parameters seem to have a negligible impact during the summer. However, the impact from Melt1 and Melt2 dominate during the wintertime when there is a

19

domain-wide change in hub-height wind speed. However, unlike LB, the impacts from Melt1 and Melt2 are unclear, as the change in WS100 is positive over certain areas but becomes negative elsewhere. In addition, the impact is not restricted to regions with snow and ice cover. This suggests that the physical processes influencing the simulated WS100 are nonlinear and the associated impact is nonlocal. As for SH (Figure 17), LH (Figure 18), and GH (Figure 19) fluxes, only Melt1 and Melt2 produce significant changes during the winter. In general, increasing Melt1 leads to decreases in surface energy fluxes over snow cover regions over evergreen forest whereas responses from increasing Melt2 is a bit ambiguous. Unlike WS100, simulated responses from Melt1 and Melt2 are restricted to the snow-cover extent. Note that there seems to be a sharp gradient over the steep slope where the response of the variable completely switches sign. This indicates that there is a lot of uncertainty for simulating near-surface variables over areas of terrain slope. Thus, more observations are needed for model validation and parameter calibration over such regions. Similar responses are also true for LST (Figure 20) and T2 (Figure 21). One additional note is that there seems to be a relatively weak domain-wide increase in LST associated with parameters of thermal conductivity during the summer. However, such impact is not apparent for T2.
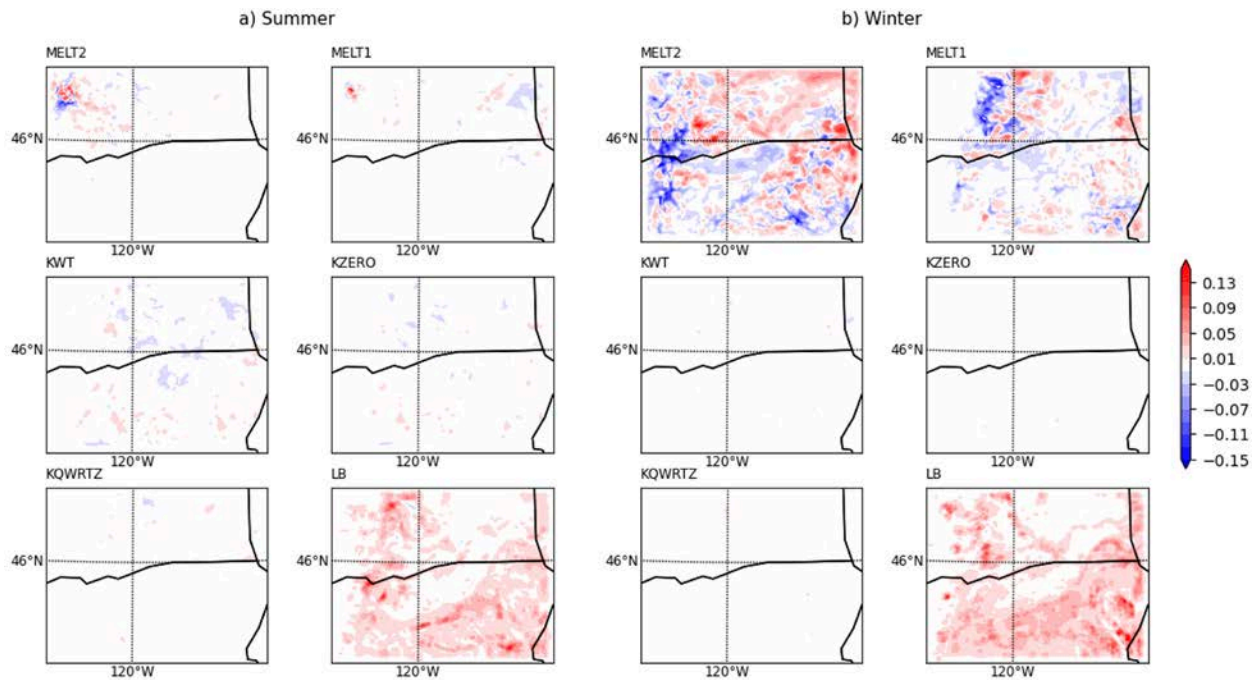
Figure 16. Spatial distribution of the responses of wind speed (m.s^{-1}) for the six most significant parameters for both the (a) summer and (b) winter periods
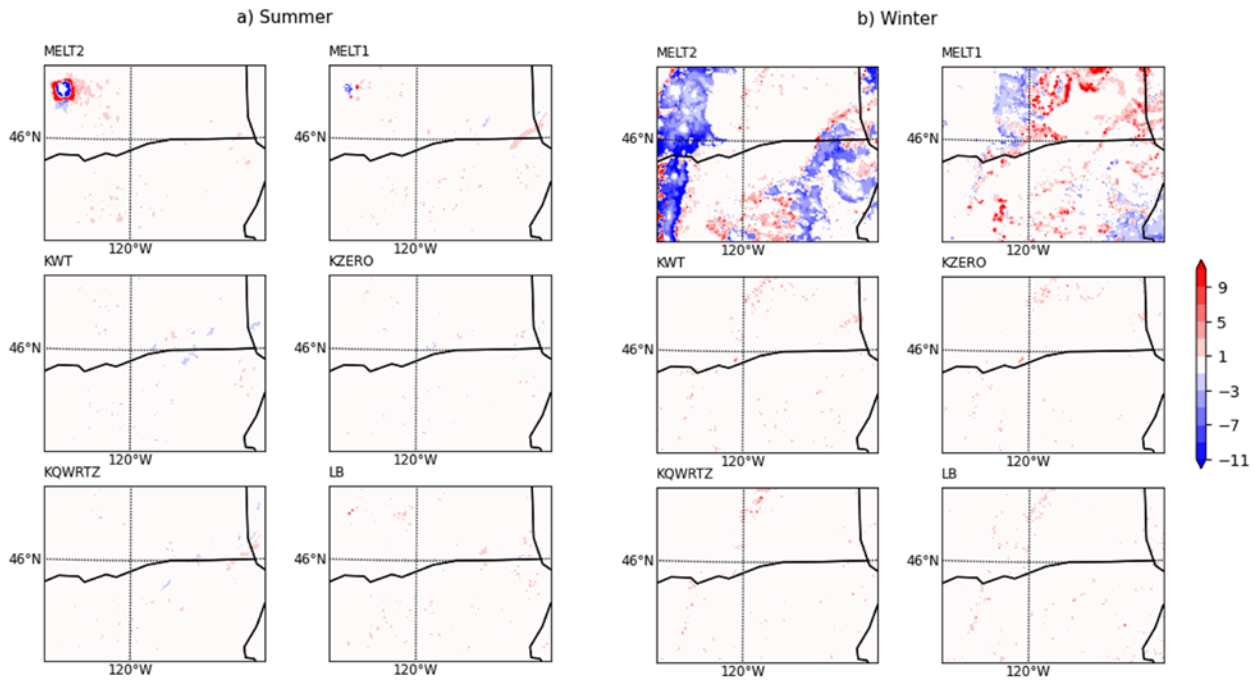
Figure 17. Same as Figure 16 but for the responses of SH flux (W.m^{-2})
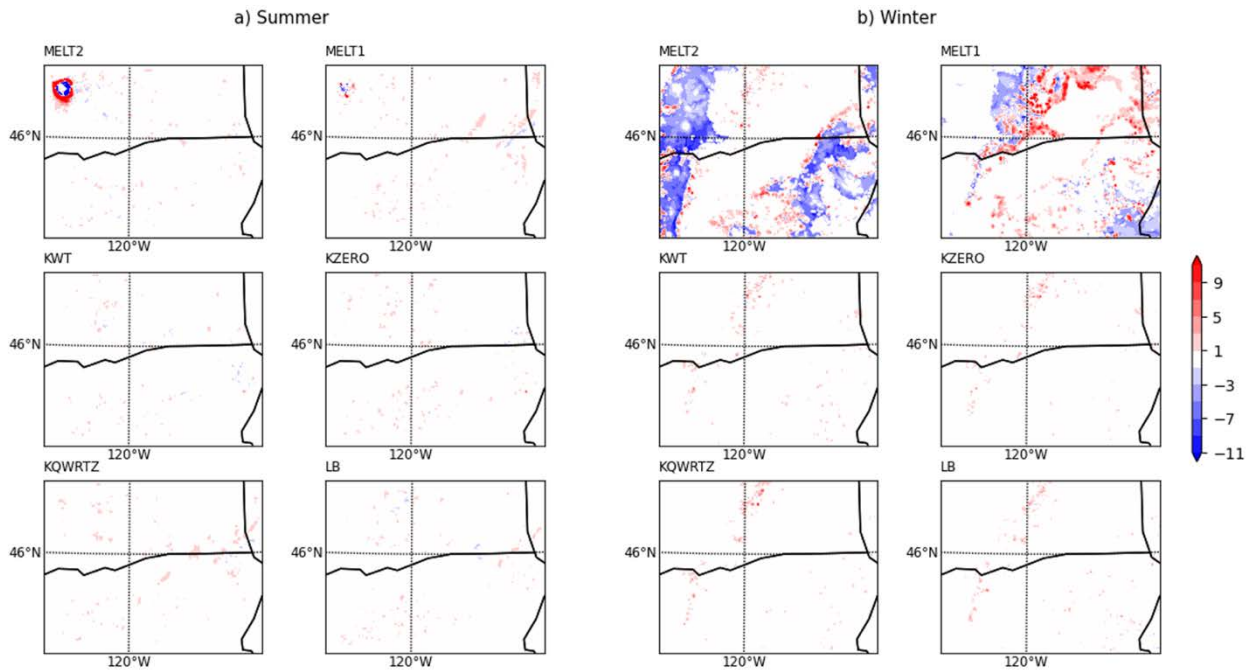
Figure 18. Same as Figure 16 but for the responses of LH flux (W.m^{-2})

21
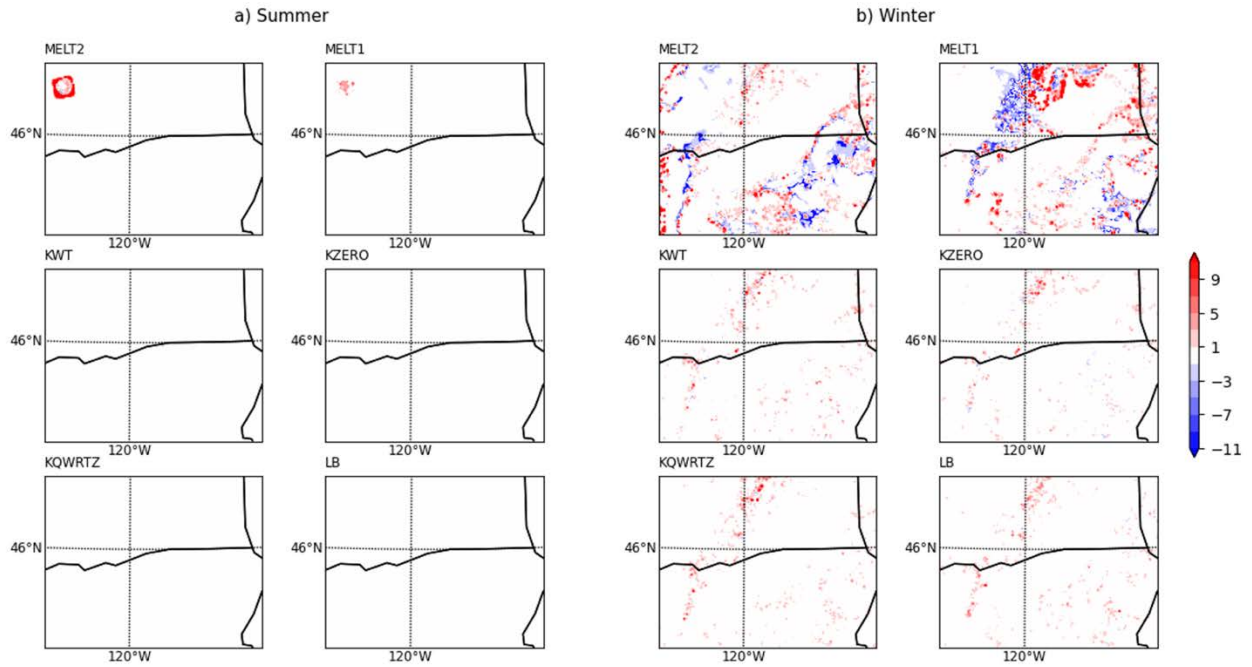
Figure 19. Same as Figure 16 but for the responses of GH flux (W.m^{-2})
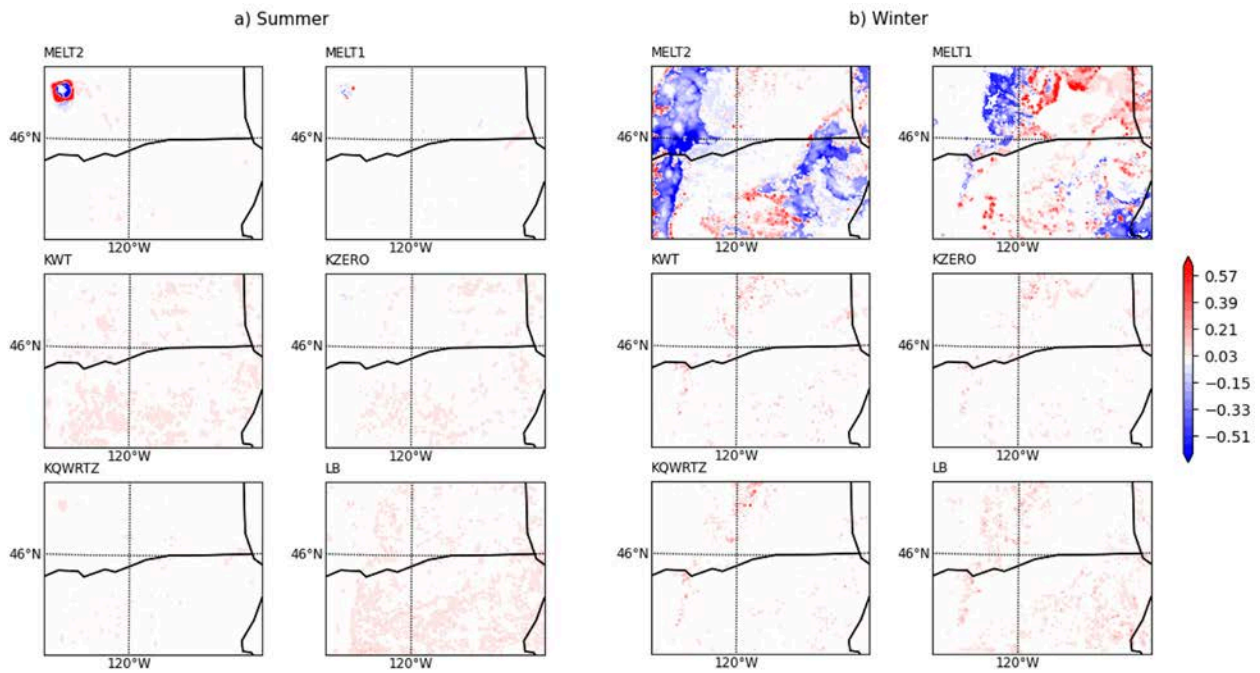
Figure 20. Same as Figure 16 but for the responses of LST (℃)
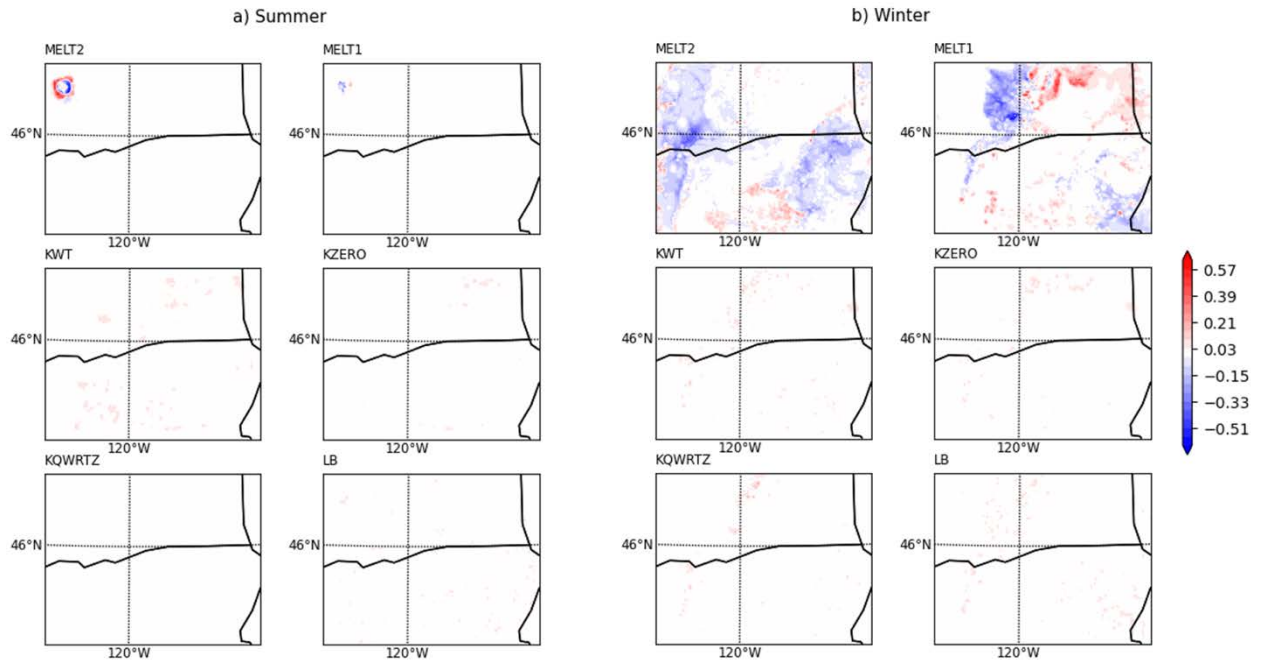
Figure 21. Same as Figure 16 but for the responses of T2 (℃)

4 Uncertainty

The preceding evaluation has identified the six most influential parameters from the RUC LSM, examined their relative dependence on land-use type and soil texture, and quantified the associated impact on the near-surface variables. However, there are still some areas that need to be discussed such as: (i) how sensitive are the results to the parameter perturbation value; (ii) is there any significant day/night contrast in terms of the relative contribution from each parameter and (iii) are there any other notable parameters that we should be aware of?

To evaluate the uncertainty of the parametric sensitivity to the perturbation value, a similar analysis is conducted using ensemble simulation from two new experiments. In the first experiment (EXP1), the perturbation range for all the examined parameters is increased to $\pm$ 50 % of the original values whereas it is reduced to $\pm$ 5% in EXP2. Because of the similarity in the figures, only results from LST are presented. Figure 22 and Figure 23 show the spatial distribution of relative contribution (%) of each parameter from both experiments during the wintertime and summertime respectively. The key contributing parameters are the same from both experiments. Note that the relative contribution of parameters associated with thermal conductivity (KWT, KZERO, and KQWRTZ) increases significantly in EXP1, especially during the summertime. This is more prominent in Figure 24, which shows the relative contribution (%) with respect to the dominant land-use types. The contribution from KWT, KZERO, and KQWRTZ add up to about 80% of the total variance in EXP1 where it is reduced to about 30% in EXP2 due to the small perturbation range (Figure is not shown for the dominant soil textures but the result is similar). As a result, the response of LST from EXP1indicates a substantial increase in surface temperature from all the thermal-related parameters (Figure 25a and Figure 26a), whereas response of surface energy fluxes is negative (figure not shown). Therefore, even though there is less uncertainty associated with the values of thermal conductivity, any potential misrepresentation can have substantial impact on the simulated surface variables.

Characterizing the day/night contrast of the parametric sensitivity for the simulated near-surface variables is not the focus of this study. However, the general conclusion can be summarized. Overall, the parametric sensitivity shows no significant day/night contrast during the wintertime period. However, during the summertime, parametric sensitivity for SH flux, T2 and LST, shows a greater day/night difference for certain parameters (e.g., KWT) in terms of spatial pattern but not magnitude. However, considering the insignificance of the relative contribution (Figures 7 and 8), the associated impact should be negligible. Other than the six identified key parameters, the only other parameter that contributes relatively more than the rest is C2SN. This parameter can be particularly sensitive to GH flux over snow cover and high-elevation regions during the wintertime.
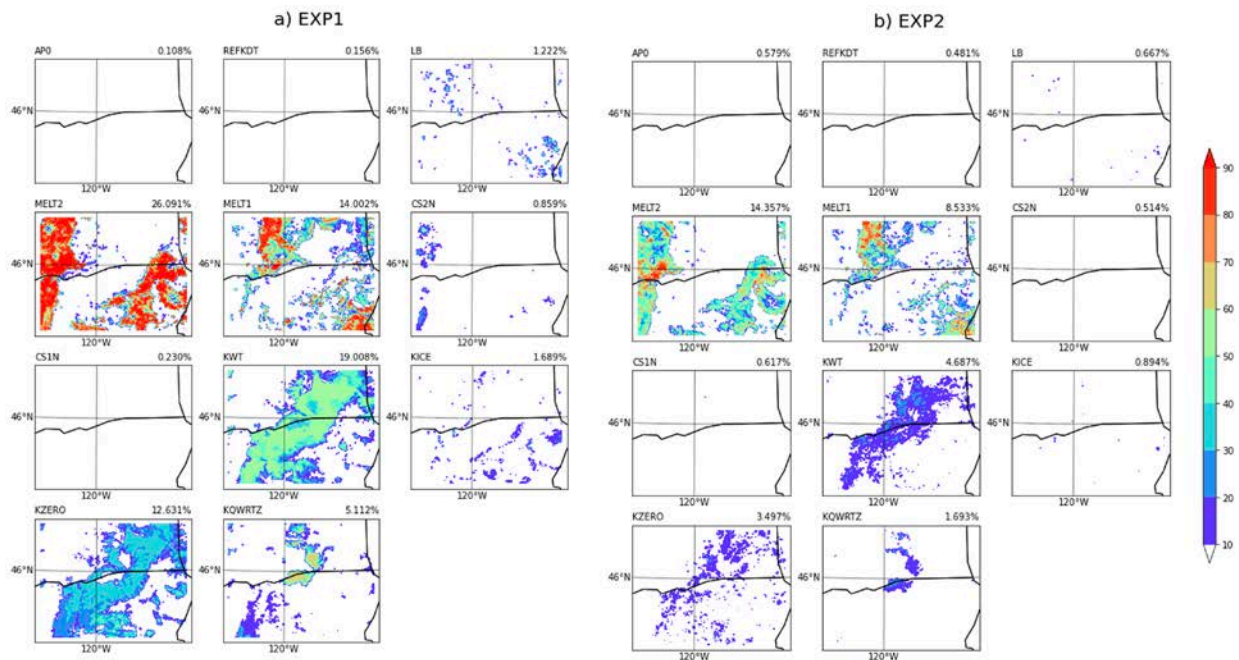
Figure 22. Spatial distributions of relative contributions (%) of each examined parameter to the total variances of the simulated LST during the wintertime from (a) EXP1 and (b) EXP2
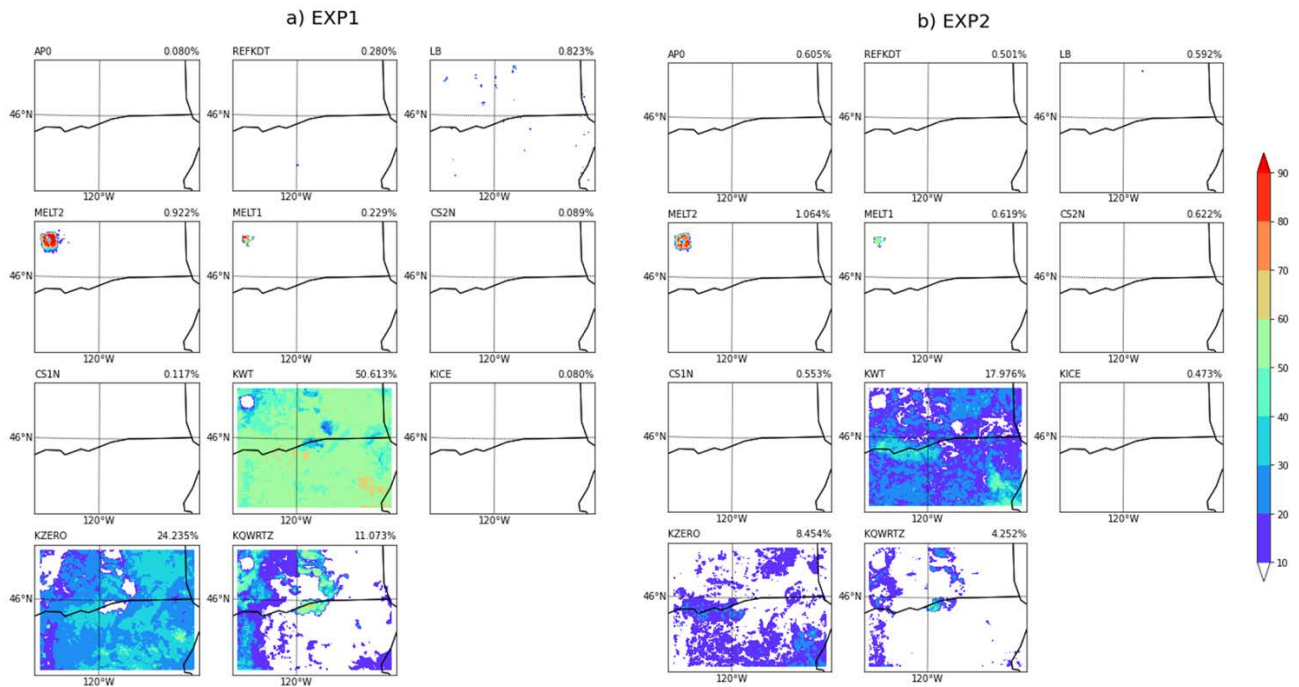
Figure 23. Same as Figure 22 but for the responses of LST (℃)
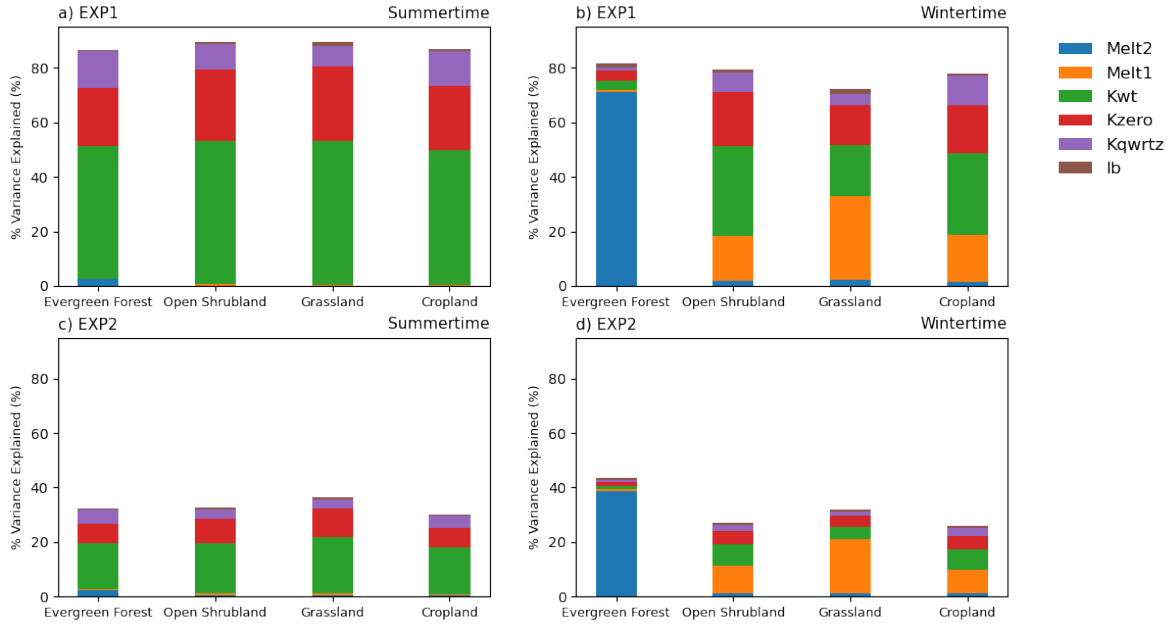
Figure 24. The relative contribution of the six key parameters (Melt1, Melt2, KWT, KZERO, KQWRTZ, and LB) to the variance of LST with respect to the four dominant land-use types (evergreen forest, open shrubland, grassland, and cropland) for both the summer (left) and winter periods from (a,b) EXP1 and (c, d) EXP2
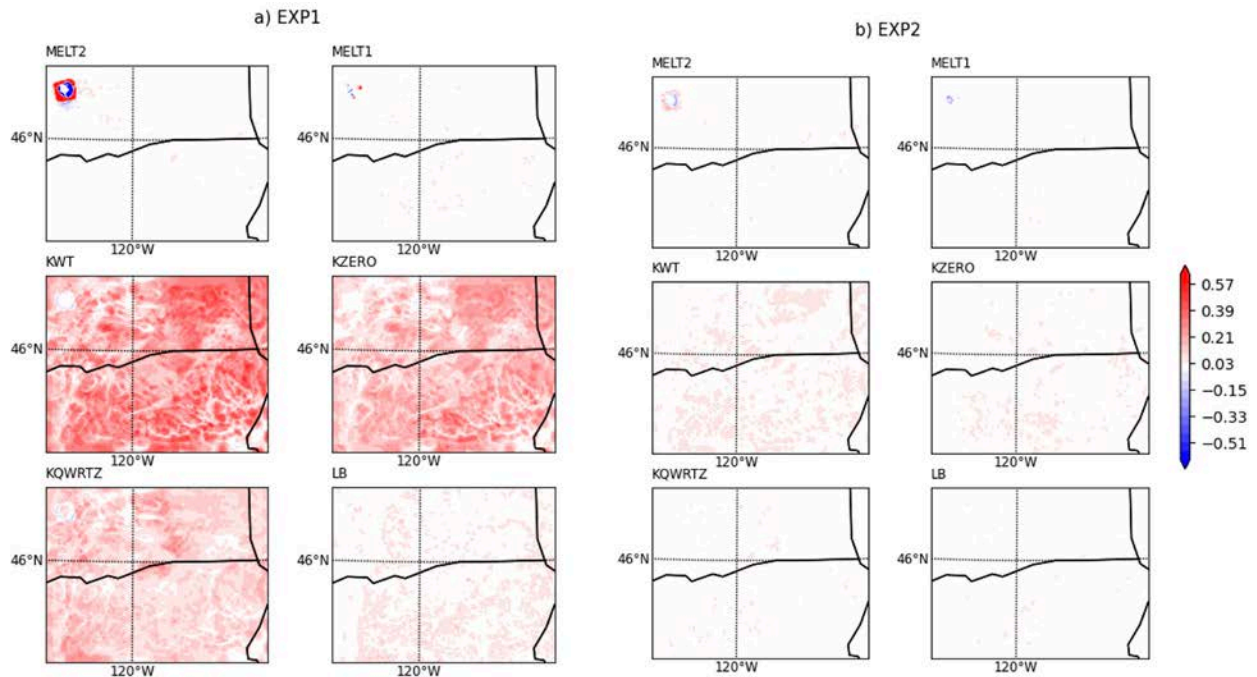
Figure 25. Spatial distribution of the responses of LST (℃) for the six most significant parameters for the summer period from (a) EXP1 and (b) EXP2

26
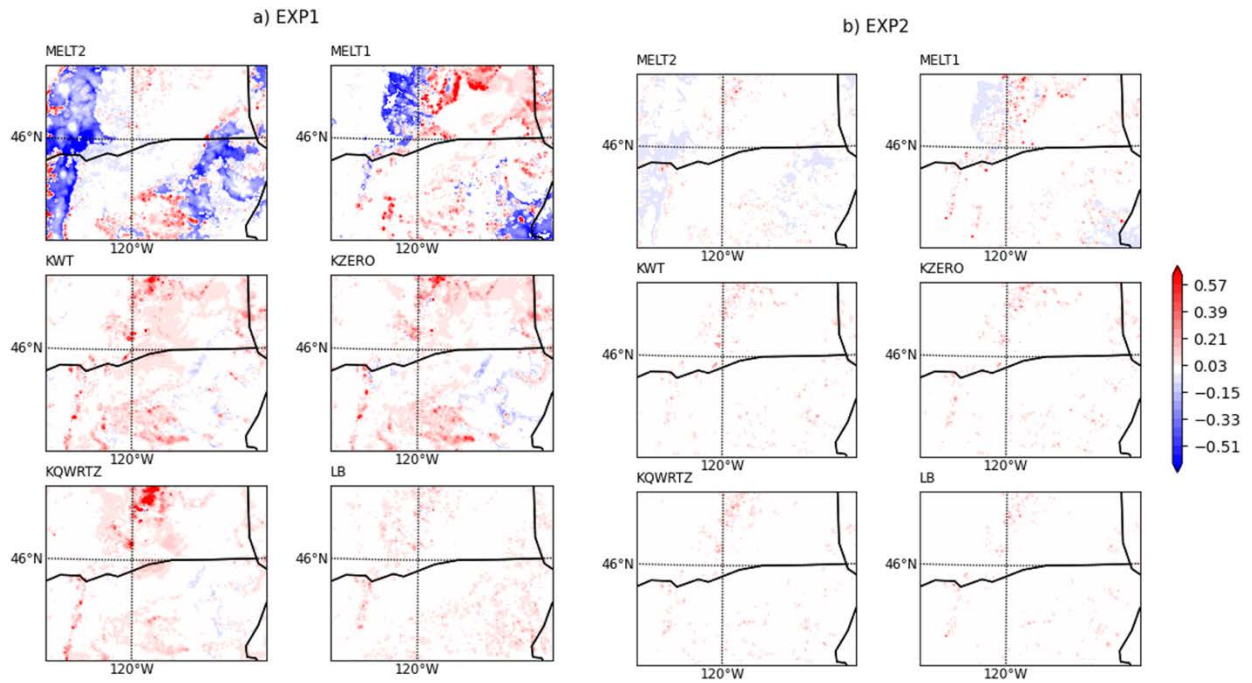
Figure 26. Same as Figure 25 but for the winter period

5 Conclusions

In this study, we investigated the parametric sensitivity of near-surface variables (e.g., SH, LH, GH, WS100, LST, and T2) to the parameters used in the RUC LSM during a wintertime and summertime periods. The RUC LSM is currently the operational land surface component used in the NOAA short-range weather prediction model over the North America domain. Therefore, understanding the parametric sensitivity in the RUC LSM would provide critical guidance for further model calibration and validation in the next generation of LSM development.

The results suggest that parameters related to snow/ice and thermal processes can have significant impact on the simulated near-surface variables. Out of the 11 examined parameters, only 6 of them (KWT, KZERO, KQWRTZ, Melt1, Melt2, and LB) have considerable influences on the model behaviors and can explain up to 60%−80% of the estimated total variance of the simulated variables. In addition, the magnitude of the parametric sensitivity varies strongly with season. For instance, parameters associated with snow/ice processes (Melt1 and Melt2) are dominant during the wintertime whereas those associated with thermal processes (KWT, KZERO, KQWRTZ) are more important during the summertime. Furthermore, the impact of the identified parameters on the simulated variables is highly related to the topography. There is a high degree of sensitivity to the parameter values over the slope region. This points out the importance of collecting field observations over steep terrain to better quantity the appropriate values of these key parameters. Interestingly, parametric sensitivity shows little dependency on the land-use type and soil category. The uncertainty analysis indicates that even though the uncertainty associated with parameters from thermal conductivity is generally small, any potential misrepresentation can have substantial impact on the simulated surface variables.

The relative importance of parameter sensitivity of RUC LSM to wind energy was also investigated by examining the impact on hub-height wind speed. Only one parameter, LB, has suggested moderate impact on the simulated hub-height wind speed. However, the associated impact on the simulated wind speed is relatively small compared to that from the PBL scheme, indicating that the impact from land surface processes on hub-height level wind is secondary as compared with the turbulent mixing from the PBL. Overall, our findings provide a better understanding of the RUC LSM behavior associated with parameter uncertainties and can be used to improve the forecasting skill of land surface processes via calibration of the most uncertain model parameters.

References

Bastidas, L. A., Hogue, T. S., Sorooshian, S., Gupta, H. V., & Shuttleworth, W. J. (2006). Parameter sensitivity analysis for different complexity land surface models using multicriteria methods. *Journal of Geophysical Research: Atmospheres*, *111*(D20). https://doi.org/10.1029/2005JD006377

Berg, L. K., Liu, Y., Yang, B., Qian, Y., Krishnamurthy, R., Sheridan, L., & Olson, J. (2021). Time evolution and diurnal variability of the parametric sensitivity of turbine-height winds in the MYNN-EDMF parameterization. *Journal of Geophysical Research: Atmospheres*, *126*(11), e2020JD034000. https://doi.org/10.1029/2020jd034000

Bianco, L., Djalalova, I. V., Wilczak, J. M., Olson, J. B., Kenyon, J. S., Choukulkar, A., et al. (2019). Impact of model improvements on 80 m wind speeds during the second Wind Forecast Improvement Project (WFIP2). *Geoscientific Model Development*, *12*(11), 4803–4821. https://doi.org/10.5194/gmd-12-4803-2019

Caflisch, R. E. (1998). Monte Carlo and quasi-Monte Carlo methods. *Acta Numerica*, 7, 1–49. https://doi.org/10.1017/S0962492900002804

Chen, F., Mitchell, K., Schaake, J., Xue, Y., Pan, H.-L., Koren, V., et al. (1996). Modeling of land surface evaporation by four schemes and comparison with FIFE observations. *Journal of Geophysical Research: Atmospheres*, *101*(D3), 7251–7268. https://doi.org/10.1029/95JD02165

Cook, D. R., & Sullivan, R. C. (2019). Energy Balance Bowen Ratio (EBBR) instrument handbook. (Rep. DOE/SC-ARM/TR- 037). Washington, DC: U.S. Department of Energy. https://www.arm.gov/publications/tech_reports/handbooks/ebbr_handbook.pdf

Findell, K. L., Gentine, P., Lintner, B. R., & Guillod, B. P. (2015). Data length requirements for observational estimates of land-atmosphere coupling strength. *Journal of Hydrometeorology*, *16*(4), 1615–1635. https://doi.org/10.1175/JHM-D-14-0131.1

Fisher, R. A., & Koven, C. D. (2020). Perspectives on the future of land surface models and the challenges of representing complex terrestrial systems. *Journal of Advances in Modeling Earth Systems*, *12*(4), e2018MS001453. https://doi.org/10.1029/2018MS001453

Guo, Z., Wang, M., Qian, Y., Larson, V. E., Ghan, S., Ovchinnikov, M., et al. (2014). A sensitivity analysis of cloud properties to CLUBB parameters in the single-column Community Atmosphere Model (SCAM5). *Journal of Advances in Modeling Earth Systems*, *6*(3), 829–858. https://doi.org/10.1002/2014MS000315

Hou, Z., Huang, M., Leung, L. R., Lin, G., & Ricciuto, D. M. (2012). Sensitivity of surface flux simulations to hydrologic parameters based on an uncertainty quantification framework applied to the Community Land Model. *Journal of Geophysical Research: Atmospheres*, *117*(D15). https://doi.org/10.1029/2012JD017521

Iacono, M. J., Delamere, J. S., Mlawer, E. J., Shephard, M. W., Clough, S. A., & Collins, W. D. (2008). Radiative forcing by long-lived greenhouse gases: Calculations with the AER radiative transfer models. *Journal of Geophysical Research: Atmospheres*, *113*(D13). https://doi.org/10.1029/2008JD009944

Johansen, O. (1975). Thermal conductivity of soils, Ph.D. thesis, University of Trondheim, Trondheim, Norway (English Translation, No. 637, Cold Reg. Res. and Eng. Lab., Hanover, NH, 1977.). https://apps.dtic.mil/sti/pdfs/ADA044002.pdf

Kain, J. S. (2004). The Kain–Fritsch convective parameterization: An update. *Journal of Applied Meteorology and Climatology*, *43*(1), 170–181. https://doi.org/10.1175/1520-0450(2004)043%3C0170:TKCPAU%3E2.0.CO;2

Kain, J. S., & Fritsch, J. M. (1990). A one-dimensional entraining/detraining plume model and its application in convective parameterization. *Journal of the Atmospheric Sciences*, *47*(23), 2784–2802. https://doi.org/10.1175/1520-0469(1990)047%3C2784:AODEPM%3E2.0.CO;2

Kenji, K. (1967) Densification of seasonal snow cover. *Physics of Snow and Ice: Proceedings*, *1*(2), 929–952. http://hdl.handle.net/2115/20351

Koren, V., Schaake, J., Mitchell, K., Duan, Q.-Y., Chen, F., & Baker, J. M. (1999). A parameterization of snowpack and frozen ground intended for NCEP weather and climate models. *Journal of Geophysical Research: Atmospheres*, *104*(D16), 19569–19585. https://doi.org/10.1029/1999JD900232

Liu, Y., Qian, Y., Feng, S., Berg, L.K., Juliano, T.W., Jiménez, P.A., & Liu, Y. (2022). Sensitivity of solar irradiance to model parameters in cloud and aerosol treatments of WRF-solar. *Solar Energy*, 233, 446–460. https://doi.org/10.1016/j.solener.2022.01.061

Mahrt, L., & Ek, M. (1984). The influence of atmospheric stability on potential evaporation. *Journal of Applied Meteorology and Climatology*, *23*(2), 222–234. https://doi.org/10.1175/1520-0450(1984)023%3C0222:TIOASO%3E2.0.CO;2

McCaffrey, K., Wilczak, J. M., Bianco, L., Grimit, E., Sharp, J., Banta, R., et al. (2019). Identification and characterization of persistent cold pool events from temperature and wind profilers in the Columbia River Basin. *Journal of Applied Meteorology and Climatology*, *58*(12), 2533–2551. https://doi.org/10.1175/jamc-d-19-0046.1

McCullagh, P., & Nelder, J. A. (1989). *Generalized linear models, second edition*. London, UK: Chapman and Hall.

Mellor, G. L., & Yamada, T. (1982). Development of a turbulence closure model for geophysical fluid problems. *Reviews of Geophysics*, *20*(4), 851–875. https://doi.org/10.1029/RG020i004p00851

Nakanishi, M., & Niino, H. (2009). Development of an improved turbulence closure model for the atmospheric boundary layer. *Journal of the Meteorological Society of Japan Ser. II*, *87*(5), 895–912. https://doi.org/10.2151/jmsj.87.895

Niu, G.-Y., Yang, Z.-L., Mitchell, K. E., Chen, F., Ek, M. B., Barlage, M., et al. (2011). The community Noah land surface model with multiparameterization options (Noah-MP): 1. Model description and evaluation with local-scale measurements. *Journal of Geophysical Research: Atmospheres*, *116*(D12). https://doi.org/10.1029/2010JD015139

Pichugina, Y. L., Banta, R. M., Bonin, T., Brewer, W. A., Choukulkar, A., McCarty, B. J., et al. (2019). Spatial variability of winds and HRRR-NCEP model error statistics at three Doppler-Lidar sites in the Wind-Energy generation region of the Columbia River Basin. *Journal of Applied Meteorology and Climatology*, *58*(8), 1633–1656. https://doi.org/10.1175/jamc-d-18-0244.1

Powers, J. G., Klemp, J. B., Skamarock, W. C., Davis, C. A., Dudhia, J., Gill, D. O., et al. (2017). The Weather Research and Forecasting Model: Overview, system efforts, and future directions.*Bulletin of the American Meteorological Society*, *98*(8), 1717–1737, https://doi.org/10.1175/BAMS-D-15-00308.1

Rosero, E., Yang, Z.-L., Wagener, T., Gulden, L. E., Yatheendradas, S., & Niu, G.-Y. (2010). Quantifying parameter sensitivity, interaction, and transferability in hydrologically enhanced versions of the Noah land surface model over transition zones during the warm season. *Journal of Geophysical Research: Atmospheres*, *115*(D3). https://doi.org/10.1029/2009JD012035

Santanello, J. A., Dirmeyer, P. A., Ferguson, C. R., Findell, K. L., Tawfik, A. B., Berg, A., et al. (2018). Land-atmosphere interactions: The LoCo perspective. *Bulletin of the American Meteorological Society*, *99*(6), 1253–1272. https://doi.org/10.1175/BAMS-D-17-0001.1

Schaake, J. C., Koren, V. I., Duan, Q.-Y., Mitchell, K., & Chen, F. (1996). Simple water balance model for estimating runoff at different spatial and temporal scales. *Journal of Geophysical Research: Atmospheres*, *101*(D3), 7461–7475. https://doi.org/10.1029/95JD02892

Shaw, W. J., Berg, L. K., Cline, J., Draxl, C., Djalalova, I., Grimit, E. P., et al. (2019). The Second Wind Forecast Improvement Project (WFIP2): General overview. *Bulletin of the American Meteorological Society*, *100*(9), 1687–1699. https://doi.org/10.1175/bams-d-18-0036.1

Skamarock, W. C., & Klemp, J. B. (2008). A time-split nonhydrostatic atmospheric model for weather research and forecasting applications. *Journal of Computational Physics*, *227*(7), 3465–3485. https://doi.org/10.1016/j.jcp.2007.01.037

Smirnova, T. G., Brown, J. M. & Benjamin, S. G. (1997). Performance of different soil model configurations in simulating ground surface temperature and surface fluxes. *Monthly Weather Review*, *125*(8), 1870–1884, https://doi.org/10.1175/1520-0493(1997)125%3C1870:PODSMC%3E2.0.CO;2

Smirnova, T. G., Brown, J. M., Benjamin, S. G., & Kenyon, J. S. (2016). Modifications to the Rapid Update Cycle Land Surface Model (RUC LSM) available in the Weather Research and Forecasting (WRF) model. *Monthly Weather Review*, *144*(5), 1851–1865. https://doi.org/10.1175/MWR-D-15-0198.1

Smirnova, T. G., Brown, J. M., Benjamin, S. G., & Kim, D. (2000). Parameterization of cold-season processes in the MAPS land-surface scheme.*Journal of Geophysical Research: Atmospheres*, *105*(D3), 4077–4086. https://doi.org/10.1029/1999JD901047

Thompson, G., & Eidhammer, T. (2014). A study of aerosol impacts on clouds and precipitation development in a large winter cyclone. *Journal of the Atmospheric Sciences*, *71*(10), 3636–3658. https://doi.org/10.1175/JAS-D-13-0305.1

Thompson, G., Field, P. R., Rasmussen, R. M., & Hall, W. D. (2008). Explicit forecasts of winter precipitation using an improved bulk microphysics scheme. Part II: Implementation of a new snow parameterization. *Monthly Weather Review*, *136*(12), 5095–5115. https://doi.org/10.1175/2008MWR2387.1

Vaisala. (2015). Triton remote sensing systems: Comparing accuracy with collocated met towers. Vaisala white paper. https://www.vaisala.com/e

Wang, C., Qian, Y., Duan, Q., Huang, M., Berg, L. K., Shin, H. H., et al. (2020). Assessing the sensitivity of land-atmosphere coupling strength to boundary and surface layer parameters in the WRF model over Amazon. *Atmospheric Research*, 234, 104738. https://doi.org/10.1016/j.atmosres.2019.104738

Wilczak, J. M., Stoelinga, M., Berg, L. K., Sharp, J., Draxl, C., McCaffrey, K., et al. (2019). The Second Wind Forecast Improvement Project (WFIP2): Observational field campaign. *Bulletin of the American Meteorological Society*, *100*(9), 1701–1723. https://doi.org/10.1175/bams-d-18-0035.1

Xia, G., Draxl, C., Berg, L. K., & Cook, D. (2021). Quantifying the impacts of land surface modeling on hub-height wind speed under different soil conditions, *Monthly Weather Review*, *149*(9), 3101–3118. https://doi.org/10.1175/MWR-D-20-0363.1

Xia, G., Draxl, C., Raghavendra, A., & Lundquist, J. K. (2021): Validating simulated mountain wave impacts on hub-height wind speed using SoDAR observations. *Renewable Energy*, 163, 2220–2230. https://doi.org/10.1016/j.renene.2020.10.127

Yang, B., Berg, L. K., Qian, Y., Wang, C., Hou, Z., Liu, Y., et al. (2019). Parametric and structural sensitivities of turbine-height wind speeds in the boundary layer parameterizations in the Weather Research and Forecasting model. *Journal of Geophysical Research: Atmospheres*, *124*(12), 5951–5969. https://doi.org/10.1029/2018jd029691

Yang, B., Qian, Y., Berg, L. K., Ma, P.-L., Wharton, S., Bulaevskaya, V., et al. (2017). Sensitivity of turbine-height wind speeds to parameters in planetary boundary layer and surface-layer schemes in the Weather Research and Forecasting model. *Boundary-Layer Meteorology*, 162, 117–142. https://doi.org/10.1007/s10546-016-0185-2

Zhao, C., Liu, X., Qian, Y., Yoon, J., Hou, Z., Lin, G., et al. (2013). A sensitivity study of radiative fluxes at the top of atmosphere to cloud-microphysics and aerosol parameters in the community atmosphere model CAM5,*Atmospheric Chemistry and Physics*, 13, 10969–10987. https://doi.org/10.5194/acp-13-10969-2013